School of Chemistry

Functionalised Diamond Surfaces using a Tube Furnace

Gurjosh Singh Barn

This thesis is submitted in partial fulfilment of the requirements for the Honours Degree of MSci (Bsc) at the University of Bristol

Supervisor: Professor Paul W May

Second Assessor: Professor Neil Fox

Physical and Theoretical Chemistry

Acknowledgements

First, I would like to that my supervisor, Professor Paul May, for giving me the guidance I needed throughout the project, and for looking over every part of my literature review and results and discussion, over the span of many different emails.

Secondly, I would like to thank Ramiz Zulkharnay, who carried out the acid cleaning and boron-doped diamond deposition layer of the diamonds.

Thirdly, I would like to thank everyone in the University of Bristol CVD Diamond Lab, who helped commissions the tube furnace.

Lastly, I would like to thank myself, simply for teaching myself how to use CasaXPS and deconvolute XPS data, when nobody else could teach me.

RKB NI SJM

Contents

Abbreviations

XPS: X-ray photoelectron spectroscopy

NEA: Negative electron affinity

PEA: Positive electron affinity

TEC: Thermionic energy converter

LEED: Low-energy electron diffraction

UPS: Ultraviolet photoelectron spectroscopy

SCD: Single crystal diamond

CVD: Chemical vapour deposition

HPHT: High-pressure high-temperature

NV: Nitrogen vacancy

sccm: Standard cubic centimetres per minute

Abstract

Diamond is a wide band-gap semiconductor (5.47 eV) that is known for its chemical inertness and its strength. These properties can be exploited for applications in thermionic energy converters (TEC's). Altering the functional groups present on the surface of the diamond can have a varying effects on the electron affinity of the diamond surface. Previous studies indicate that a metal oxide termination of diamond produces a favourable negative electron affinity (NEA), which increases the rate of thermionic emission of electrons from the diamond. Many methods of diamond surface oxidation such as O_2 plasma treatment result in an inhomogeneous layer of oxygen on the surface, as oxygen can bond in many different configurations such as carbonyl (C=O), ether (C-O-C), or hydroxyl (C-OH). This initial oxygen termination before subsequent metal termination produces a range of NEA values across the diamond surface, emphasising the need for a method to produce a homogenous oxide layer. Water vapour annealing using a tube furnace gave a promising abundance of OH-termination on the surface of SCD diamond (100). This method was also used to attempt to achieve an N-terminated diamond, which could be used in place of the oxide layer in metal-oxide termination, however it was unsuccessful, as confirmed by analysis of all diamond samples with X-ray photoelectron spectroscopy (XPS).

Introduction

Thermionic Energy Converters

Thermionic energy converters (TEC's) generate energy through the thermionic emission of electrons from a heated source emitter. Shown in **Figure 1** is a schematic diagram of a TEC; the emitter is heated causing electrons to thermionically emit from the surface, into vacuum. The electrons are collected by a cooled collector, and due to the difference in work function between the emitter and the collector, when the two are connected, a potential difference is generated, and a load is driven. The collected electrons will flow back into the emitting materials. Also shown between the emitter and collector is the space charge region, which occurs when some thermionically emitted electrons do not have sufficient kinetic energy to travel across the vacuum gap and reach the collector, so they accumulate in the space-charge region, forming a 'virtual cathode', repulsing other thermionically emitted electrons and reducing the efficiency of the TEC. This problem can be fixed with the addition of low-pressure caesium vapour, or gases such as H_2 and CH_4. The temperature required for thermionic emission from a given material can be defined by the Richardson-Dushman**.** equation **(equation 1)**[1]. An extensive review of TEC's will not be discussed further.

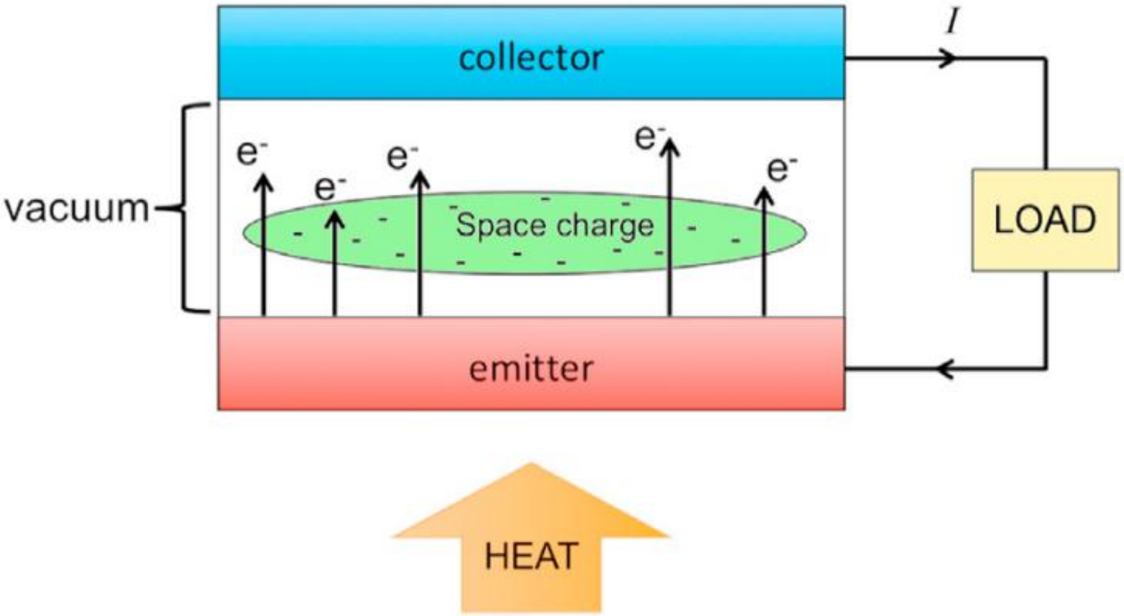

Figure 1 Schematic diagram of a thermionic energy converter (TEC)[1]

$$J(T) = A_R T^2 \exp\left(-\frac{\phi}{kT}\right) \textbf{(1)}$$

J=Emission current density (A cm^{-2})

A_r=Richardson constant (material specific)

Φ=Work function

k=Boltzmann constant

Altering the surface chemistry of diamond significantly affects the thermionic emission pathway of electrons, and studies have shown that a scandium oxide-terminated diamond is the most promising termination for TEC applications. In order to create a metal oxide terminated diamond, the diamond must first be terminated with a homogenous oxygen layer, then a subsequent metal layer. The problem arises with the initial oxygen termination; oxygen can bond to the surface of the diamond by multiple different configurations, yielding an inhomogeneous oxide layer, that has inconsistent electronic properties across the surface. This paper reviews the method of water vapour annealing to achieve a fully OH-terminated diamond, that could be functionalised via wet chemistry creating complete ketone or ether coverage

Properties of Diamond

Repeating units of sp^3 hybridised carbon atoms make the well-known allotrope, diamond. Though many may assume its use is limited to make precious jewellery and increasing the hardness and durability of power tools, functionalising the surface chemistry of diamond can have multiple applications in the electrochemical field, particularly when making thermionic energy converters (TEC). Termination of the surface of single crystal CVD diamonds using various species such as oxygen and nitrogen can increase the energy of the conduction band minimum, so that it is higher in energy than the vacuum level, creating a negative electron affinity (NEA) on the surface of the diamond. This creates an alternative emission pathway for electrons where there is no emission barrier to overcome, so electrons are readily emitted from the surface of the diamond.

Diamond possesses a face-centred cubic (FCC) crystalline structure, as depicted in **Figure 2A.** The consistency of the covalently bonded sp^3 carbon atoms give diamond its characteristic hardness. Within the crystalline structure, various planes are present, each of which have varying stabilities. For example, based on the Wulff criterion for crystal habit, the octahedral (111) face is the most thermodynamically stable plane in diamond, followed by the cubic (100) and (110) faces[2] shown in **Figure 2B**. Additionally, studies show that the (111) plane has the least amount of strength and therefore the least amount of energy required to create the cleavage compared to other planes within the crystalline structure[3]. For such reasons, dominance of the (111) plane is observed on the surface of many natural diamond samples. This is not the case for synthetic diamond grown by methods such as chemical vapour deposition (CVD) or high-pressure, high temperature (HPHT), which have a dominance of the (100) plane due to solvent effects[4, 5].

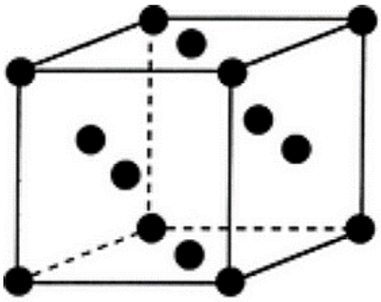

Figure 2A Face-centred cubic (FCC) structure of diamond[113]

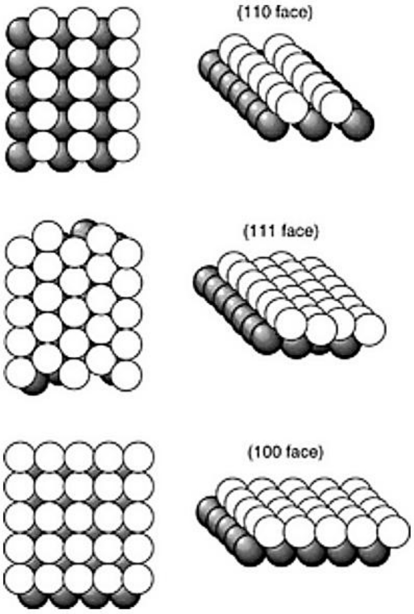

Figure 2B Surface planes of diamond[113]

The surface of the given planes may have different reactivities with regards to gas-surface interactions, due to the varying number of dangling bonds (unpaired electrons) present on the surface. For example, the (111) plane has 1 dangling bond, unlike the (100) plane which has 2 dangling bonds, creating the assumption that the (100) plane would have increased reactivity compared to its (111) counterpart. However, this assumption fails to account for the energy-lowering surface reconstruction, resulting in a the (100) plane turning into a 2 × 1 surface. This same reconstruction can occur for the (111) plane at higher temperatures and is otherwise known as a Pandey chain reconstruction[6].

Semiconductor's, NEA's and PEA's

A semiconductor is a term that describes a substance whose electrical conductivity increases proportional to temperature. In a semiconductor, when T=0, the valence band (VB) is full, and the Fermi level (E_F) lies directly above this band **(Figure 3)**. The conduction band (CB), which does not contain any electrons at this temperature, lies higher in energy and is separated by a band gap. Increasing the temperature of this material allows electrons at the top of the valence band to be thermally excited across the band gap, into the conduction band.

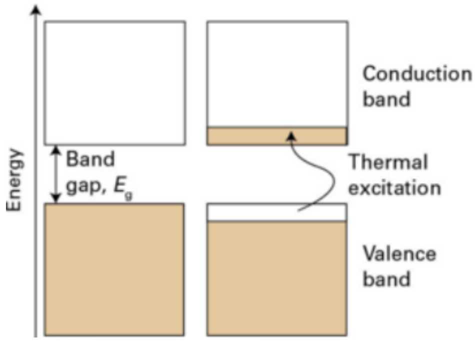

Figure 3 (a) band structure of a semiconductor at T=0, where no thermal excitation occurs, and the material does not conduct electricity. (b) T>0, thermal excitation of electron occurs, and the material begins to conduct electricity.[7]

This means that the material now has electrical conductivity which can be increased with temperature, as the rate of thermal excitation of electrons increases[7].

Diamond is classed as a wide bandgap semiconductor, with a bandgap of 5.47 eV, indicating that it is useful for high temperature conductivity applications, due to its low intrinsic carrier density[8]. Altering the surface chemistry of the diamond enables the fine-tuning of its electronic properties, dependant on the species that terminates the surface. Terminating the surface with a species that has a higher electronegativity than carbon will cause the surface to possess a positive electron affinity (PEA), and termination with a less electronegative species will create a negative electron affinity (NEA).

The work function (ϕ) of a material can be described as the energy barrier to free space that prevents an electron at the Fermi level from escaping a solid[9]; this changes dependant on whether the material presents with an NEA or a PEA **(Figure 4)**. NEA surfaces of diamond are of great interest due to their ability to provide an alternative emission pathway, where the conduction band minimum (CBM) is higher in energy than the vacuum level (E_{vac}). In this scenario any electrons in the conduction band have no emission barrier to overcome to be emitted from the surface, therefore electrons in the valence band would only need to be excited into the conduction band to be emitted from the surface of the diamond[1].

In some instances, electrons have an additional energy barrier to overcome before escaping the surface and being emitted into vacuum; this is known as the electron affinity (χ). If the electron affinity is negative, the conduction band minimum is significantly high and lies above the vacuum level, without the need for band bending. This is called a 'true' NEA, or otherwise known as an intrinsic NEA[1]. An effective NEA is a result of the band bending that occurs at the surface of p-type semiconductors, where the conduction band is pulled above the vacuum level due to charge redistribution. Electrons that are excited into the conduction band of the diamond can either become trapped in the surface conduction band minimum by thermalising, or tunnel through the barrier to be emitted into vacuum, which is lower than that of a true NEA surface[1]. Most semiconductors will exhibit a PEA surface, where the Fermi level will remain between the valence band and the conduction band. Typically, the energy of the vacuum level will reside higher than that of the CBM, so that electrons will have an additional energy barrier to overcome before they can be emitted from the surface into the vacuum[1,10].

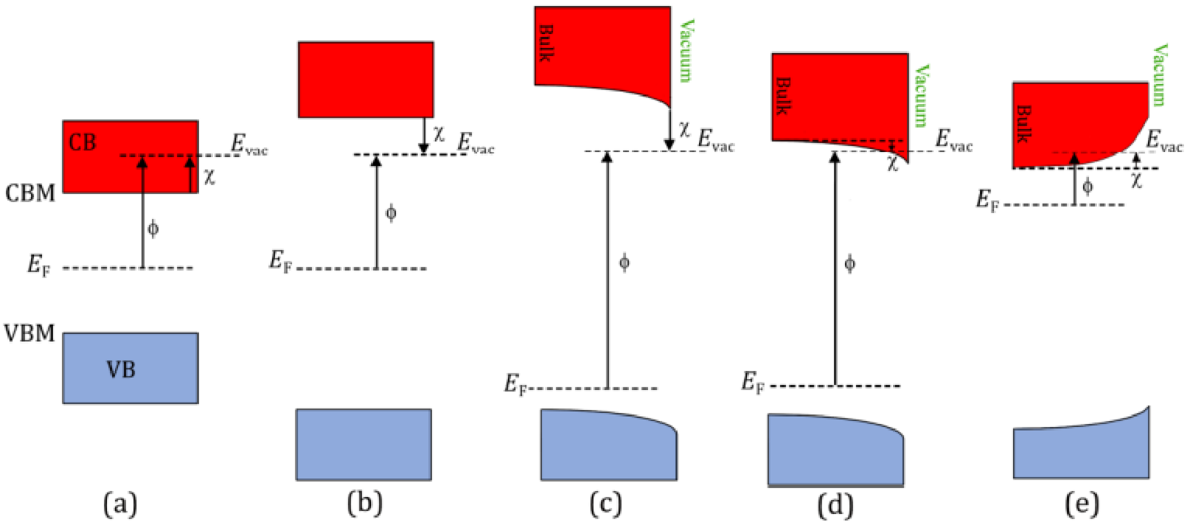

Figure 4 (a) PEA, (b) true NEA, (c) p-doped material exhibiting an NEA with downward band bending (d) effective NEA with downward band bending (e) PEA in an n-doped material exhibiting upward band bending.[1]

The electronic behaviour of diamond can also be altered by introducing impurities (known as ‘dopants’) into the crystal lattice structure[11]. P-type diamonds are typically made by growing diamond and adding boron-containing gases into the gas mixture in either a microwave or in a hot filament reactor. Boron can also be implemented into the diamond by ion-implantation[12] followed by annealing to remove radiation damage and driving the dopant into the desired lattice sites[13]. P-type doping results in an increase in the number of electron-accepting positively-charged ‘holes’ present in the lattice as the dopant is more electron deficient than carbon. In many cases, boron is used. This increase in the number of positively-charged ‘holes’ present in the diamond, which act as charge carriers, creating a subsequent increase in the diamond electrical conductivity.

Opposed to p-type doping, n-type doping involves introducing chemical species that have an abundance of electrons, such as nitrogen or phosphorous, into the crystal lattice structure of the diamond. N-type doping can also be performed by ion implantation[14] and development of n-type doping by CVD growth of diamond is currently being researched[15]. The increased number of electrons present in the diamond due to the presence of the dopant can be supplied to the conduction band of the doped material, hence increasing its conductivity[16]. N-type doping will result in an upward band bending at the diamond surface, which induces a PEA. However, this can reduce or prevent electron emission, therefore p-type doping of diamond is typically more favourable when there is significant downward band bending in tandem with a large NEA. These conditions create a smaller energy barrier for electron to be excited and emitted[1].

Various diamond terminations

Amine- Termination

Amine-Terminated diamond can be generated by exposing H-terminated diamond to ammonia plasma generated by a radio-frequency plasma chamber, using customized parameters consisting of quartz tube surrounded by a 3-turn RF coil, connected to an impedance- matching network and a 13.56 MHz RF source. To ensure complete amino-termination of the surface, samples can be protonated in concentrated hydrochloric acid for one minute and dried under a gentle nitrogen flow, to protonate any N-terminations formed from the fragmentation of amino-terminations[17]. Amine-terminations on the surface of the diamond are defined as chemical functional groups that contain one N atoms with three single bonds to any combination of H and C atoms. In a study conducted by D. Zhu et al[17] XPS measurements determined that the primary amino groups were the most stable, and most readily protonated into -NH_3^+ configuration of amine that terminated the surface of the nanodiamond. UPS measurements of -NH_2 and -NH_3^+ (formed by treatment of -NH_2-terminated diamond with HCl) showed that both samples showed exhibit an NEA surface. A sharp peak at the low-kinetic-energy of the photoemitted electrons is characteristic of an NEA surface **(figure 5)**, as electrons excited from the valence band of the diamond, into the conduction band quasi-thermalise into the conduction-band minimum and are then emitted into vacuum[18].

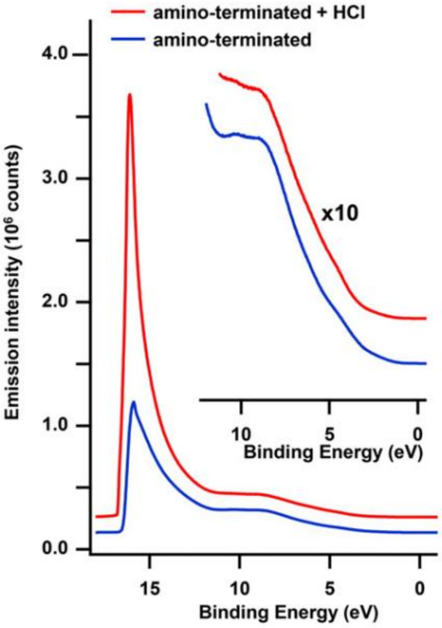

Figure 5 UPS Spectra of NH_2-terminated (amino-terminated) diamond and NH_3^+ (amino-terminated + HCl), showing a sharp peak at the lower end of the binding energy, inferring a low kinetic energy, charecterising the diamonds NEA surface.[17]

Aminated diamond surfaces are of great interest in the biomedical field, particularly in biosensing applications. Biomolecules such as proteins and DNA have an abundance of amino acids, which can be linked to the surface of the aminated diamond, as the amine group is biocompatible with the molecules[19]. Studies conducted by Artemenko *et al*[20] concluded that NH_3 RF plasma treatment of O-terminated and H-Terminated nanocrystalline diamond resulted in a small amount of in situ primary amine surface termination. Per 100 surface C atoms, 1.3 and 0.8 primary amine moieties were detected on the surface of H-terminated and O-terminated diamond, respectively. Though many studies aim to achieve a full monolayer coverage of diamond with various functional groups, for biosensing applications, having space between amine moieties on the surface of the diamond is important to allow room for large biomolecules. However, amine-termination using RF plasma treatment does result in an overall decrease in surface conductivity in both O- and H-terminated diamond. O-terminated diamond is already classified as non-conductive, however, termination with an amine moiety further decreases the diamonds surface conductivity, as determined by I-V measurements. This effect is consistent with the surface termination of H-terminated diamond, which shows a drastic drop in conductivity from 10^{-5} S to 10^{-12} S, after functionalisation[20].

In the same study by Artemenko et al[20], amination of NCD diamond was successfully achieved by coating the NCD with a thin amine-containing plasma polymer. Using this method, O-terminated diamond remained non-conductive, and amine-containing plasma polymer treatment of H-terminated diamond did reduce the conductivity of the diamond, but only by two orders of magnitude from $\sim 10^{-5}$ S to $\sim 10^{-7}$ S, This indicates that preservation of surface conductivity is more likely to be achieved by amine-containing plasma polymer treatment, when comparing both methods.

Maintaining suitable levels of surface conductivity of diamond is extremely important for bioelectronic applications such as electrochemical sensing for DNA, glucose, dopamine and uric acid[21]. In particular, amine-terminated diamond can be used as chemical transducers to confirm successful grafting of odorant binding proteins (OBPs) to artificially mimic the human olfactory system. Electrochemical impedance spectroscopy (EIS) was used in Manai's et al[22] study to confirm that odorant binding proteins can be successfully attacked to the surface of amine-terminated diamond. EIS relies on the flow of electric current in the bulk and interfacial region of the material[23], emphasising the importance of keeping the surface conductivity of diamond for bioelectronic applications.

Fluorine- and chlorine- termination of Diamond

Typically, termination of a diamond surface with fluorine is achieved by various plasma treatment methods, however these techniques can often have damaging effects on the diamond. Y-F. Wang *et al*[24] developed an electrochemical technique that involves configuring H-terminated diamond into a MISFET structure and applying an electrical field perpendicular to a thin layer of LiF that is on the diamond, which resulted in a F-terminated diamond surface[24]. Fluorine-termination of diamond (110) results in in a PEA surface, as it has a higher electronegativity than carbon, directing the dipole moment away from the surface. This property, combined with an absence of surface related inter bandgap states, and an absence of surface electron spins, make fluorine-terminated diamonds a strong contender for NV-based quantum sensors[25].

Chlorination of the diamond surface is typically a lot more challenging than fluorination, as chlorine is less reactive and has a larger atomic radius compared to fluorine[25]. Functionalising a diamond surface with chlorine can be achieved by thermal annealing under chlorine, followed by a photo-assisted, or thermally-assisted amination step[26]. Chlorine-termination does result in a relatively weak PEA surface (0.96-0.98 eV), however extensive research is not conducted on such terminations due to its lack of applications[27]. Studies show that chlorination of the diamond surface often results in an increase in surface roughness by approximately 1 nm in comparison to the previously non-functionalised (100) oriented diamond, rendering it useless for real-world applications[29].

Boron- and Boron nitride- termination of diamond

Govindaraju et al[30] conducted a study with the aim of forming a boron termination of the surface of nanodiamonds, with the utilisation of electrophilic boron precursors with OH-terminated diamond. The study involved placing nanodiamond into a tube furnace and aerobically oxidising the samples at 525°C for 5 hours, then drying the samples to ensure the complete removal of water. The diamond samples were then reacted with various trigonal boron precursors such as boron tribromide and boron trichloride and left to react for between 1-24 hours. Samples were then purified by centrifugation and subjected to analysis. The results did not indicate that a full monolayer coverage of boron was achieved, however, C-B bonds were formed, alongside many other impurities.

Density functional theory studies conducted by Shen *et al*[27] indicate that diamond surface functionalisation with boron can either exhibit a NEA or PEA surface, depending on whether the surface is oxidised or bare. Adsorption of boron onto bare diamond creates an NEA surface, however adsorption onto an oxidised surface creates a PEA. This is due to the fact that adsorption of boron onto a bare diamond surface causes a dipole moment, favouring electron emission, creating a NEA surface. Oxygen is more electronegative (3.44) than both carbon and boron therefore, O atoms become negatively charged when placed between C and B, which induces a dipole moment that increases the electron emission barrier, resulting in a PEA surface.

BN- surface terminations can have varying effects on diamond depending on the configuration of the bonding of the BN moiety to the diamond surface[31]. DFT calculations conducted by Shen *et al*[27] show that BN can bond to the surface of the diamond as (C)-N-B or as (C)-B-N which produce a PEA and NEA surface, respectively.

Metal-oxide termination of diamond

Computational studies of metal-oxide-terminated diamond conducted by O'Donnell *et Al.*[33] suggest that lighter alkali metal-oxide terminations, such as LiO- or MgO- terminations, produce a stronger NEA surface than heavier alkali metal-oxide terminations such as CsO- or KO- terminations. Theoretical calculations show that a monolayer coverage of Li and half monolayer coverage of Mg on an oxygenated 2 x 1 unit cell surface show an NEA of -3.50 eV and a range between -3.50 and -2.18 eV respectively. The strongest calculated NEA values of KO- and CsO- terminated diamond were found to be -2.44 eV and -2.41 eV, indicating that lighter alkali metal-oxide terminations may be better suited to thermionic emission applications. Experimental studies conducted by O'Donnell *et Al.*[34] of Mg adsorption onto an oxidised surface are somewhat in line with previous theoretical calculations of MgO- terminated diamond surfaces, yielding an NEA of -2.0 eV. It should be noted that DFT calculations will often vary from experimental calculations, as DFT often neglects on-site coulomb repulsion, leading to an incorrect prediction of metal behaviour for small band gap systems[34].

Experimental studies of TiO terminated diamond showed promising NEA values, with a maximum NEA of -0.9 eV. Comparing TiO termination to other similar metal oxide terminations such as ScO, SnO, and AlO indicates that SnO is the least promising termination for TEC applications due to the desorption of SnO at temperature above 700-800 °C, however, it did show a maximum NEA value of -1.37 eV at half monolayer coverage. TiO and AlO yielded similar NEA values, with AlO exhibiting a maximum NEA value of -1.0 eV. Both terminations also exhibited similar work function values of ~4.5 eV, with a small work function being highly favourable. However, TiO terminated diamond undergoes an unexplained phenomenon, where at high temperatures, 90% of oxygen coverage is lost at temperatures >800°C, despite oxygen termination being stable up to 900 °C, and TiO_2 being stable up to >1800 °C. No literature was found to explain this phenomenon, however it is suspected that a surface reconstruction occurs at higher temperatures, resulting in O atoms migrating to the surface[35].

Recent studies conducted by Zulkharnay *et al* [36] indicate that ScO is the most promising metal-oxide termination for TEC applications. ScO-terminated diamond (100) is thermally stable up to temperatures of 700 °C, and produces a large NEA value of -1.02 eV, with a small work function of <3.63 eV[36]. However, aforementioned terminations such as TiO and AlO may be cheaper alternatives for TEC applications.

H-termination

Due to the nature of CVD diamond growth, CVD diamonds are naturally H-terminated[37]. On the (111) surface, 1 hydrogen atom will bond to the single available dangling bond available per carbon, producing a subsequent repeating row of H atoms pointed perpendicular to the surface **(Figure 6A)**. Opposingly, due to the partial overlap of H atoms on the (100) surface when two hydrogen atoms bond to the two dangling bonds on each carbon, it is energetically favourable for a surface reconstruction to occur to form (2 × 1) dimer rows[38] **(Figure 6B)**.

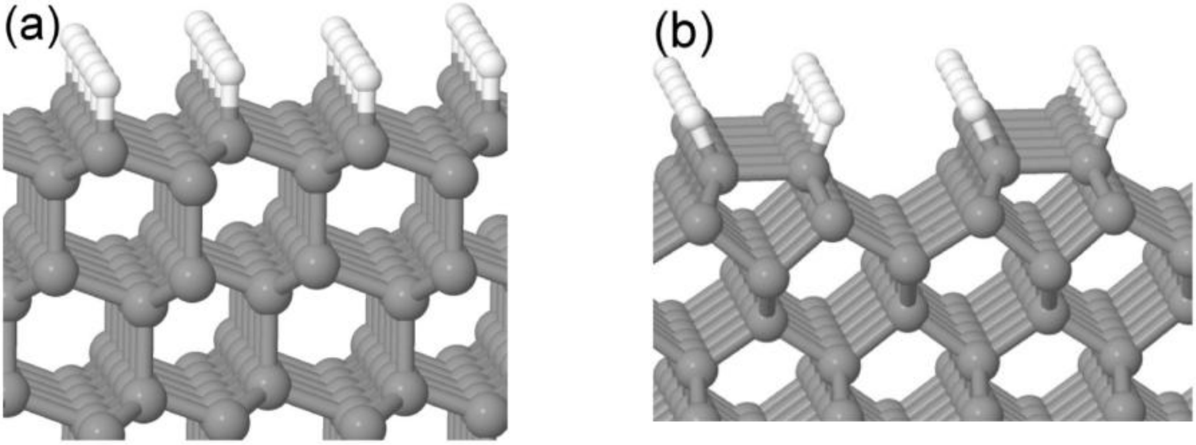

Figure 6 (a)(111) surface of diamond, (b)(100) surface of diamond. White atoms represent hydrogen, grey atoms represent carbon atoms.[1]

Hydrogen is slightly less electronegative than carbon, therefore surface termination of diamond with hydrogen creates a surface dipole, where the bulk of the diamond is partially negative, and the hydrogen layer is partially positive. Repulsive forces in the negative bulk, paired with the attractive forces of the positive surface cause electrons to be attracted to the surface of the diamond, and then emitted. In this scenario, and other similar scenarios, the diamond can be described as having a negative electron affinity (NEA), as the vacuum level is equal or below the conduction band minimum[1]. It is this NEA that gives H-terminated diamond p-type surface conductivity[39].

Ab initio studies of the (111) and (100) surface plane of hydrogen were conducted, and two different geometries of the (100) surface were used in the calculations. It is agreed that the (111) surface displays a symmetric Pandey chain reconstruction, and that the (100) surface is most stable in a 2 × 1 reconstruction in the diamonds natural state. This theory is sustained for the (111) surface following a hydrogen termination, however the (100) surface exhibits varying stabilities dependant of the orientation (shown in **Figure 7**) of the surface dihydrogen. In the symmetric configuration where the hydrogen atoms are symmetric along the crystallographic axis created a very close interatomic distance between the two hydrogens of 1.10 Å, resulting in a increased repulsion between the atoms, deeming it to be energetically unfavourable. In the twisted configuration, the hydrogen atoms maintain the same height above the carbon surface but have a slight twist to avoid the repulsion between the hydrogen atoms. This resulted in a reduction of the surface energy by 7 meV per surface carbon in comparison to the symmetric structure. The most favourable configuration was the canted configuration, where each hydrogen atom tilts away from the crystallographic axis, resulting in a H-H distance of 1.38 Å. This configuration lowered the surface energy by 0.42 eV per surface carbon, concluding that the canted geometry is the most stable (100) hydrogen-terminated diamond plane[40].

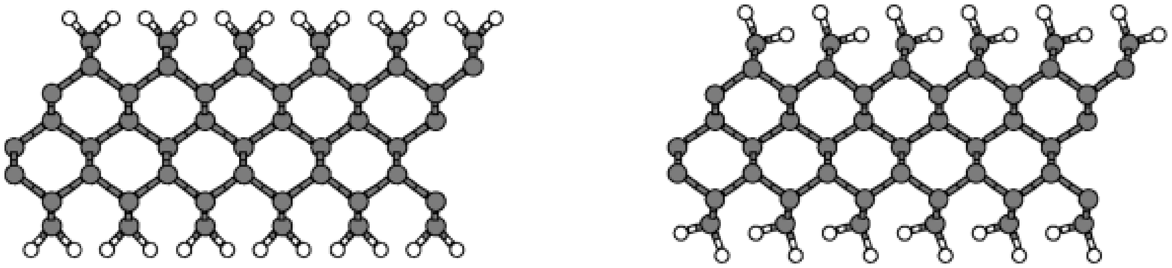

Figure 7 (left) symmetrical orientation of hydrogen-terminated (100) plane, (right) canted orientation of hydrogen-terminated (100) plane[40]

Accumulation of a hole layer in the subsurface of hydrogen-terminated diamond gives the diamond its p-type conductivity and the ability to support a high charge carrier density of 4 x 10^{13} cm^{-2}, resulting in a high electrical conductivity. Current densities along different diamond surfaces vary due to the areal density of the dipole moment from C-H bonds being 20-30% higher in high Miller-indexed surfaces such as the (111) and (110) planes in comparison to the (100) surface[41]. For such reasons, preferential hydrogen etching on the (111) and (110) planes may be considered over the (100) plane, for electrochemical applications to improve conductivity.

Conductivity of hydrogen-terminated diamond surfaces shows an environmental dependence, which can best be described by a theory called the transfer doping mechanism[42]. The mechanism describes the movement of electrons from the valence band of the bulk diamond to acceptor sites in an aqueous atmospheric layer. The surface of hydrogen-terminated diamond has a low ionization energy of 4.2 eV, enabling an energetically favourable interaction between hydronium ions in the moisture layer on the diamond surface. **Equations 2 and 3** explains the redox reaction that occurs at the moisture layer on the surface of hydrogen-terminated diamond.

$$Diamond \rightarrow Diamond^{2+(holes)} + 2e^{-} \; (2)$$

$$2H_3O^{+} + 2e^{-} \rightarrow \; H_2 + 2H_2O(3)$$

This reaction creates the hole accumulation at the surface of the diamond, enhancing its surface conductivity. By creating reasonable assumptions about the partial pressure of hydrogen in the atmosphere and the acidity of the moisture layer, Ristein[43] yielded an 'atmospheric window' which refers to the range of chemical potentials for electrons in the moisture layer on the surface of the diamond under atmospheric conditions. The window ranged from -4.44 and -4.12 eV, which refers to the range of electron energies by which electron transfer to aqueous electrolytes such as H_3O^+, from hydrogenated diamond, is thermodynamically feasible. The study states that the valence band maximum of diamond (-4.2 eV) falls directly within this window, therefore supporting the theory of the transfer doping mechanism of electron transfer from the surface of hydrogen-terminated diamond to aqueous hydronium ions in the moisture layer.

N-termination

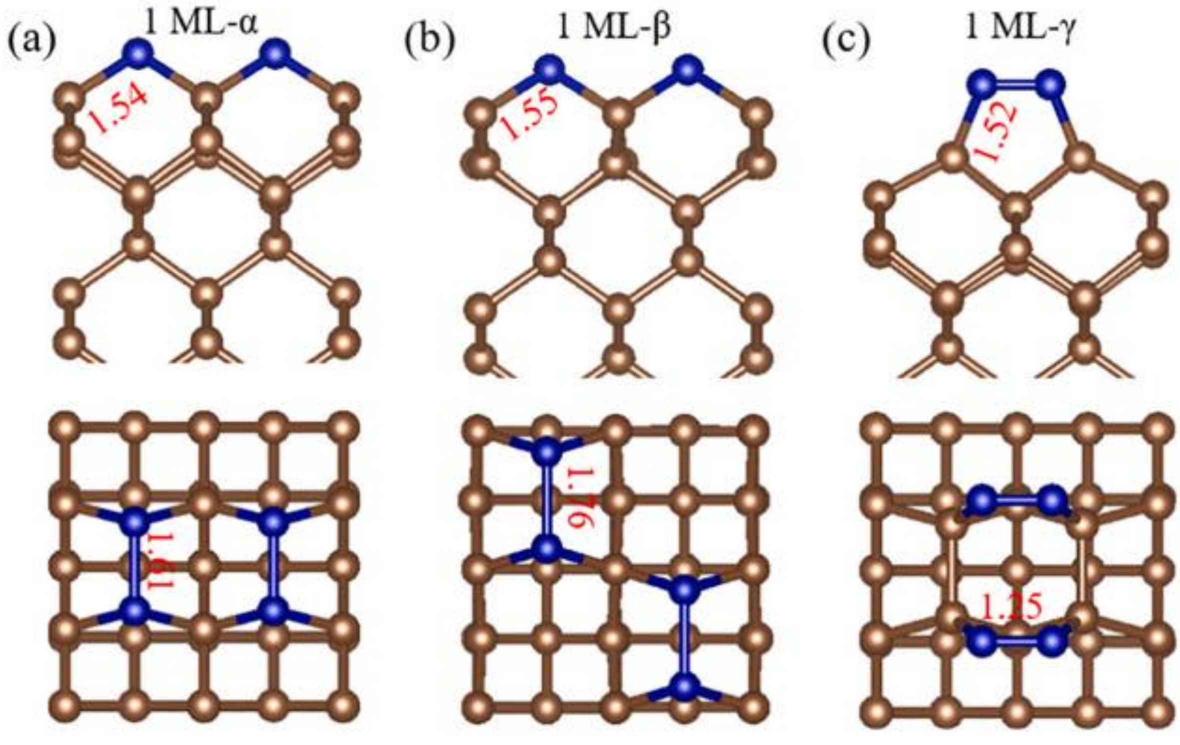

Figure 8 Configurations of nitrogen-terminated diamond (100), and their associated bond lengths[45].

Similar to O-terminated diamonds, N-terminated diamonds exhibit a PEA surface, when H-terminated diamond is replaced by N at values greater than a 0.5 monolayer coverage[44], due to nitrogen's increased electron affinity in comparison to carbon. However, *ab initio* studies conducted by Gong *et al* [45], determined that diamond (100) surface reconstructions with 1 monolayer (ML) coverage are stable over the entire chemical potential range. Three configurations of diamond surface 1ML N-terminations were calculated: ML-α, ML-β, and ML-γ **(Figure 8).** The ML-α structure consists of the N atom forming C-N-C bonds with two of the diamond surface carbon's, with a reported bond length of 1.54 Å, and two adjacent N atoms form a bond of length 1.61 Å. The ML-β configuration shows a staggered N dimer configuration on the diamond (100) surface, with bond lengths of 1.55 Å and 1.76 Å for the N-C and N-N bonds respectively. The ML-γ structure causes the surface C atoms to reconstruct into C dimers, and the N atoms form bonds with the carbon atoms at a length of 1.52 Å. Finally, the adjacent N atoms form stronger bonds with bond lengths of 1.25 Å[45].

Some diamonds contain nitrogen vacancy centres **(Figure 9)**, which can either occur naturally when diamond is harvested from the Earth, or if the diamond is grown in the presence of nitrogen using techniques such as high-pressure high-temperature (HPHT) synthesis[46]. A nitrogen vacancy (NV) centre in diamond consists of a nitrogen atom substituting a carbon atom near a missing carbon atom in a diamond crystal[47]. The nitrogen vacancy can accept an electron from its surrounding environment, causing it to be negatively charged, creating multiple energy levels in the diamond's bandgap. These energy levels correspond to two electronic configurations: a S=1 ground state and an optically active S=1 excited state, with an excitation energy of less than that of diamond (5.47 eV)[47].

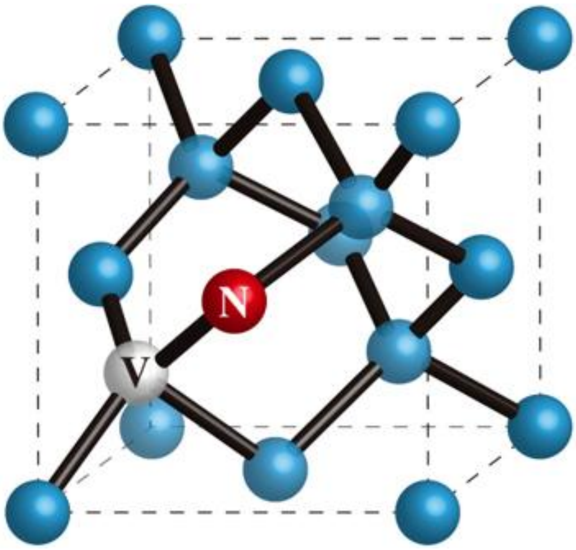

Figure 9 Nitrogen Vacancy in diamond.[114]

A negatively charged nitrogen-vacancy has many quantum applications such as information processing and metrology[48]. Altering the surface chemistry of a diamond with species such as nitrogen can affect the stability of NV centres that are close to the surface of the diamond[49]. Shallow nitrogen vacancies fail to retain spin coherence, which negatively affects their ability as a quantum sensor to monitor magnetic fields[50]. Additionally, shallow centres also show instability, indicated by photoluminescent studies[51]. Studies conducted by Chou *et al*[44] indicate that by terminating the surface of the diamond with nitrogen the, NV centres can be stabilised. Spin coherence of shallow NV centres degrade within 100 nm of the surface of the diamond due to defects on the surface of the diamond, such as dangling bonds, that lead to noise that obscures the sensing target[44,52]. By terminating the surface of the diamond with nitrogen, these dangling bonds no longer affect the spin coherence times of the NV centres.

However, it is plausible to conclude that any chemical species is capable of terminating dangling bonds on the surface of the diamond, and hence improve the spin coherence times of the NV centre. However it is the PEA surface that stabilises the NV^- centre that makes nitrogen one of the most suitable species for NV^- stabilisation. Oxygen and fluorine termination also create PEA surfaces, however O- and F- termination of diamond commonly increases surface roughness and stabilise defects with unsaturated bonds on the surface which contribute to surface-induced spin noise[44].

Additional functionalisation of a nitrogen-terminated diamond surface can have applications in molecular sensing[53]. For example, nitrogen-terminated surfaces can be further functionalised with the addition of amine groups, which would allow for amide-bond formation by EDC/NHS (N-(3-dimethylaminopropyl)-N'-ethylcarbodiimide hydrochloride/N-hydroxysuccinimide) coupling chemistry with molecules containing carboxylic acid functional groups. Amine-sulfhydryl crosslinking is also plausible for amine-terminated diamond, with molecules that contain thiol groups, such as cysteine. The ability of a nitrogen-terminated surface to produce a stable anchoring point for additional species makes it highly desirable for biosensing applications for proteins or DNA[53].

O-termination

Contrary to H-terminated diamond surfaces, O-terminated surfaces yield a positive electron affinity (PEA) due to the noticeable increase in electronegativity for oxygen in comparison to carbon. A resultant dipole moment directed away from the diamond surface significantly reduces or completely prevents electron emission, compared to a H-terminated surface[54]. Oxygen can bond to the surface of diamond in multiple different orientations, each of which have a varying effect on the electrochemical properties of diamond. Shown in **Figure 10** are some of the most common ways that oxygen can bind to the surface of oxygen (hydroxyl group C-OH, ether group C-O-C, carbonyl group C=O, and peroxide group C-O-O-C)[55].

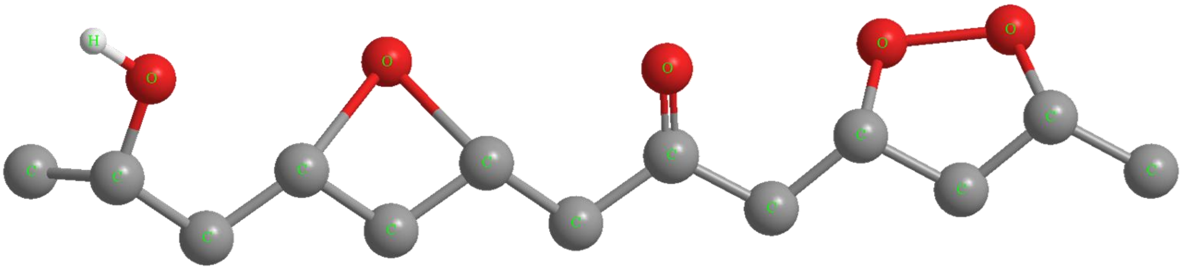

Figure 10 Orientations of oxygen termination on the surface of diamond (from left to right) hydroxyl configuration, ether configuration, carbonyl configuration, peroxide configuration.

Most of these orientations can be classed into two categories: 'oxygen on top' (O_{ontop}), where oxygen atoms bond directly to individual surface carbon atoms, which includes the carbonyl group, or oxygen can form an 'oxygen bridge' (O_{bridge}), which includes the ether and peroxide configurations. DFT calculations show that OH- termination has a significantly different effect on the extent of interfacial electron transfer in comparison to other O-terminating configurations. OH- termination of diamond shows a significantly high rate of electron transfer to atmospheric adlayers which contain oxidative species such as O_2, O_3, and H_3O^+. For example, OH-termination showed a partial electron transfer of 1.44e to the water + O_2 + H_3O^+ adlayer, in comparison to O_{ontop} and O_{bridge} which showed a partial electron transfer of 0.22e and -0.02e respectively. The presence of these oxidative species increases the intensity of electron transfer from the diamond to the surface adlayer due to the proton transfer mechanism that occurs between the hydrogens on the terminal OH's and the hydronium ions present in the adlayer, which react to form water and hydrogen molecules. This proton transfer occurs alongside electron transfer, creating a redox reaction; OH- terminating species donate protons and electrons, and the oxidative species in the adlayer act as acceptors, and are reduced in the process. This redox reaction is energetically favourable, and therefore the rate of electron emission from the bulk diamond to the surface is highly efficient[56].

Additional DFT calculations were conducted by Petrini and Larsson[57] to investigate the theoretical energetic stability and geometry of H- and O- terminated diamond (100) surfaces. Studies show that hydrogen-terminated diamond surface is energetically stable, however they are less favourable than oxygen terminations. H- terminations have an adsorption energy of -4.30 eV per adsorbate, unlike oxygen terminations which show an adsorption energy of -5.95 eV (ketone), and -6.21 eV (ether) per adsorbate. Based on the given information, the ether configuration is the most stable, however, this adsorption energy for the ether configuration is only achievable at a surface coverage of >50%, when cross-dimer bonding improves. Therefore, it is appropriate to conclude that oxygen-termination of diamond in the carbonyl configuration is the most energetically favourable at low surface coverage, but ether configurations are the most energetically favourable at higher surface coverages (>50%).

Earlier studies by Zheng and Smith[58] show that stability of oxygen on the diamond surface is dependent on the diamond surface reconstruction, the coverage level and the adsorption site. For example, on the (111) diamond plane at half-monolayer coverage, the ether configuration is the most stable (7.94 eV per oxygen atoms), unlike at monolayer coverage, where the peroxy bridge configuration is the most stable (6.21 eV per oxygen atoms). On the (100) plane, with half-monolayer coverage, the most stable configuration results in a 2 × 1 ether configuration, which supports the reconstructed diamond surface. However at monolayer coverage, with a 1 × 1 topology, two stable configurations with very similar chemisorption energies are exhibited. In the carbonyl configurations, a calculated chemisorption energy of 8.57 eV per oxygen atom is observed, and the ether configuration shows a chemisorption energy of 8.43 eV per oxygen atom. However, oxygen molecules preferentially dissociate, leading to atomic configurations; the most stable transitional configuration is oxygen in its molecular form on dimer bridge sites, leading to the evolution of the 1 × 1 atomic carbonyl model[58].

Oxygen-terminated diamond is often used to create metal oxide terminations on the surface of diamond, for applications in thermionic energy converters (TEC's). The concept of a metal oxide terminated diamond was explored in a previous section, but the justification of the initial oxygen-termination will be discussed in this section. Depositing metal directly onto a non-functionalised diamond surface is not plausible for all metals, due to their inability to form bonds with carbon[35]. *Ab initio* studies of the deposition on lithium onto the surface of unmodified H-terminated diamond indicate that an NEA is a plausible possibility, however lithium shows a weak bond strength when directly bound to carbon, exhibiting a C-Li bond length of >2 Å when bound to the C(100)-(2 × 1) surface[59]. Metals can successfully form M-

O bonds with oxygen; therefore, an oxygen layer is often used as the ‘sticking’ layer for metals to bond to the surface of diamond **(figure 11)**. Such terminations successfully produce an NEA surface with a high thermal stability and a low work function[60].

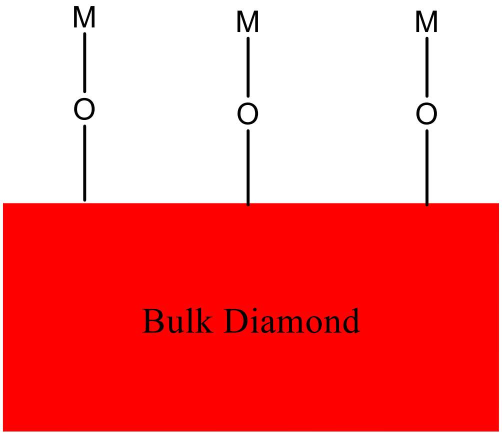

Figure 11 Schematic diagram of diamond surface terminated with metal oxide, using oxygen termination as 'sticking' layer, where ‘M’ is a metal.

OH-termination

There is a limited amount of experimental literature of OH-terminated diamond due to the difficulty of achieving a homogeneous layer of OH, without the presence of other oxygen configurations. Li *et al*[61] describes a method of diamond surface hydroxylation by hydroxide ion treatment of diamond (100) at high voltages in deionized water. Essentially, H-diamond were fixed to a platinum electrode submerged in deionized water, and a voltage of 3000 V was applied to generate hydroxide ions in the water. Although this method proves that complete OH-termination of diamond is achievable, it was not permissible without an increase in surface roughness, likely due to etching caused by increasing voltages, as indicated by atomic force microscopy (AFM) analysis. Such surface roughness creates surface inhomogeneity, possibly resulting in a variance of surface electron affinity values cross the surface of the diamond, although not explicitly reported in the paper.

Yoshida *et al*[62] described a promising technique of achieving complete OH-termination of diamond (111) by water vapour annealing, without etching the surface of the diamond. The method involves placing the diamond sample into a tube furnace which is heated to a high temperature (300-700 °C) and placed under vacuum. A flow of nitrogen bubbled through ultrapure water was fitted to one side of the furnace, creating a gaseous N_2+H_2O environment, within the tube. A schematic diagram is shown in **figure 12**. The study claims that water vapour annealing at T>500 °C results in an OH-terminated (111) diamond that is atomically flat. This method could be used to achieve a full OH-termination that could be further functionalised into a carbonyl or ether layer, for subsequent metal-oxide termination,

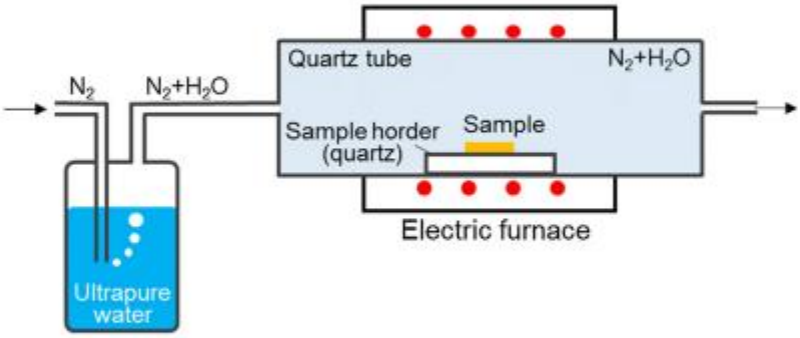

Figure 12 Schematic diagram of a tube furnace used to anneal water vapour onto the surface of diamond.[62]

Characterisation Techniques

X-Ray Photoelectron Spectroscopy

X-Ray Photoelectron Spectroscopy (XPS) is a quantitative method that is used to measure the elemental composition of the surface of a sample[63]. The method includes using either Al Kα (1486.6 eV), Mg Kα (1253.6 eV) or synchrotron-generated (variable energy) X-ray photons to photoexcite core electrons on the surface of the sample, which are then ejected and display characteristic binding energies[64]. **Equation 4** explains the relationship between the energy of the X-ray (hν), the binding energy (BE) of the electron with respect to the Fermi level, the kinetic energy (KE) of the electron emitted, and the spectrometer work function (ϕ_{spec}), which is a constant value[65]. XPS creates a spectrum with photoelectrons peaks which are labelled by the element and the orbital from which the electron was emitted from. **Figure 13** shows a schematic diagram explaining **equation 4**.

$$\mathrm{H}\nu = \mathrm{BE} + \mathrm{KE} + \ \phi\mathrm{spec}\ (4)$$

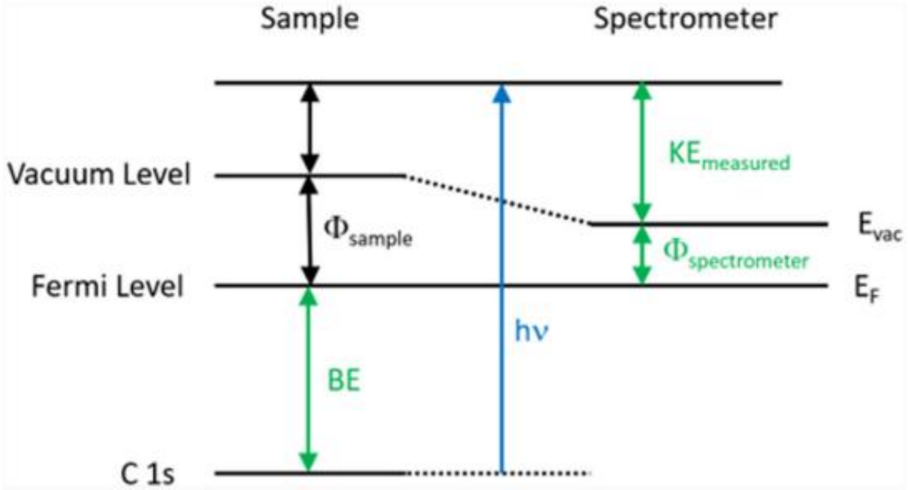

Figure 13 Schematic diagram showing the movement of electrons from the core orbital of a given element (in this case the 1s orbital of carbon) during XPS analysis)[65]

When exciting photoelectrons with X-rays, there is a possibility for the irradiated material to be ionised and be left in an excited state. This is due to the change in the potential of the sample upon creation of a 1s core-hole. Subsequently, the XPS spectrum would show an intense peak related to the original ejected photoelectron, alongside multiple peaks of a higher binding energy, due to the energy loss for excitation of electrons to higher energy bound orbitals. Such peaks are known as shake-up satellites[66].

Deconvolution of C 1s peaks in an XPS spectrum can give an indicator on the extent of surface graphitisation of diamond samples. Typically, the ratio of sp^2/sp^3 carbon on the surface of the diamond can be determined by deconvoluting the C 1s peak found at ~285 eV in the XPS spectra. This involves adding components to the region that contains the C 1s peak, and analysing their binding energies, and peak areas to determine the relative abundance of the carbon environments (components). CasaXPS[68] is a useful curve-fitting software that is often used for peak deconvolution. There are many intricacies that arise with the deconvolution of XPS peaks, specifically with the C 1s peak[69] as it is comprised of many overlapping peak signals that can have a drastic effect on the determination of surface characterisation if done incorrectly, which is why it is incorrectly reported in many papers. C 1s peaks should be properly analysed with a suitable number of components that result in a residual STD as close to 1 as possible.

Ultraviolet Photoelectron Spectroscopy (UPS)

Ultraviolet photoelectron spectroscopy (UPS) is a similar characterisation technique to XPS, however, it produces insight into the valence electronic structure of the sample being analysed. UPS involves exciting valence electrons to above the vacuum level with UV photons, which causes them to elastically reach the surface-vacuum interface. Electrons with sufficient kinetic energy will contribute to the measured spectrum, but a small fraction of these electrons will have just enough energy to reach the surface-vacuum interface via an inelastic scattering process. Hence, they are called secondary electrons. The spectrometer will detect a combination of secondary electrons and elastically scattered valence band electrons, creating the observed UPS spectrum[70].

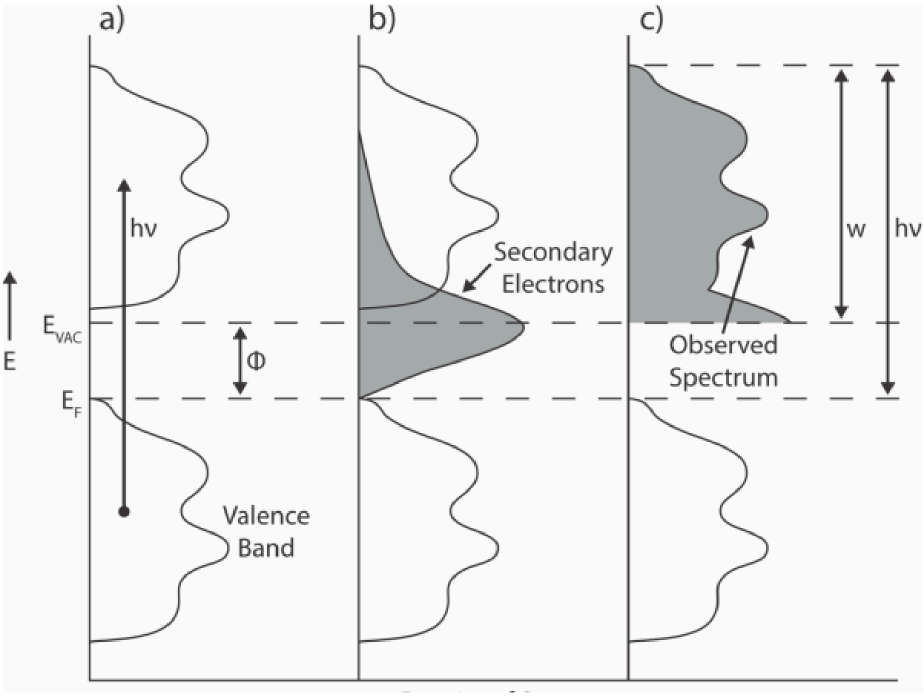

Figure 14 Schematic diagram of the processes leading to a UPS spectrum. E_f, E_{vac}, hv, ϕ, and w represent the Fermi level of the spectrometer, the vacuum level, the energy of the impinging photons, the work function, and the width of the observed spectrum respectively.[70]

UPS can be used to determine the presence of an NEA or PEA surface, which in turn can be used to confirm that a given diamond surface has been successfully functionalised with the intended chemical species. Romanyuk et al[71]. described a method of using UPS and XPS data from undoped and boron-doped polycrystalline diamond films with various surface functionalisation's to calculate the electron affinity of the surface. UPS measurements of the valence band maximum and the vacuum level were used to determine the electron affinity of the diamond samples **(Equation 5)**, to reduce errors due to spectrum edge spearing, band bending measurements collected from XPS data and the UPS spectrum vacuum level were used as an additional method of calculating electron affinity **(Equation 6)**. The two calculated values were then averaged, and electron affinities of the diamond films, as well as their respective deviations were determined.

$$\chi_1 = E_{vac} - E_{CBM} \ (5)$$

In Eq.2, E_{vac} is the energy of the vacuum level and E_{CBM} is the energy of the conduction band minimum.

$$\chi_2 = E_{vac} - (E_{VBM}^{b} + BB + E_g) \ (6)$$

In Eq.3, E_{vac} is the energy of the vacuum level, E_{VBM} is the energy of the valence band maximum, BB is the band bending magnitude, and E_g is the energy gap between the VBM and CBM.

Low-energy electron diffraction (LEED)

Low-energy electron diffraction (LEED) is an analytical technique used to determine the crystal structure of surface layers of a sample, and the co-ordinates of atoms within its respective unit cell[85]. During the process of LEED analysis, low energy electrons are used to probe the surface of the crystallographic sample, interacting with only the first few layers of atoms, as the electrons will possess an inelastic mean free path of ~5-20 Å[72]. The elastically back scattered electrons are analysed in the 20-1000 eV energy range, which make them ideal probes for the crystal surface as the interatomic spacings between surface atoms are of the same order of magnitude as the electron's de Broglie wavelengths. This leads to diffraction, given that the surface atoms are arranged periodically[73]. The elastically back-scattered electrons are then visualised as the reciprocal lattice of the samples surface on a fluorescent screen[74]. Quantitative data from the LEED analysis can be obtained by plotting incident electron energy against modulated intensities of diffracted beams[75]. These incident electrons can elastically scatter more than once, leading to the 'multiple scattering' phenomena[76].

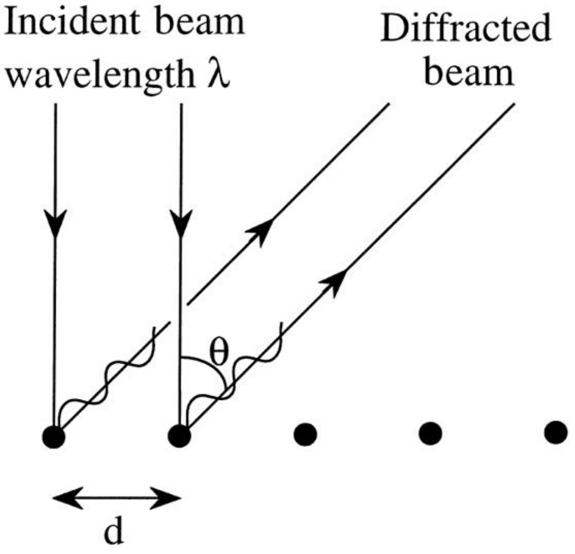

Figure 15 Low-energy electron diffraction (LEED) process. Θ is the angle between the incident beam and the diffracted beam, d is the interatomic distance[113]

LEED data can be complicated by multiple scattering, due to the complex diffraction patterns it creates[77]. To account for the multiple scattering phenomena, calculation schemes should be conducted, that normalise the scattering into a sequence of successive single scatterings[78]. Normalisation of multiple scattering into a succession of single scattering is appropriate for a clean, smooth surface; this changes in the scenario where the crystal surface is rough. In the context of this study, etching of the diamond surface is highly probable when samples undergo thermal annealing. Increasing surface disorder caused by the presence of vacancies and adatoms, increase the complexity of the subsequent computational calculations required to account of multiple scattering. Held[79] describes a method for accounting for multiple scattering using a kinematic approximation. However this approach cannot be used for rough surfaces, negating its use on potentially etched diamond surfaces. New developments in quantitative LEED data analysis, using the ViPErLEED Package[76] accounts for multiple scattering events, and has less of a reliance on user input compared to older, more established quantitative LEED analysis packages such as TENSERLEED, which require significantly more user input to account for multiple scattering events from samples that are not smooth and clean.

Essentially, surface chemical composition analysis using LEED alongside a computational quantitative calculation package such as TENSERLEED was previously a viable, however highly complicated procedure for samples that do not have a homogenous surface. The ViPErLEED package automatically accounts for multiple scattering events, which can create theoretical data that are comparable to experimental data. Consequently, ViPErLEED can be used to aid in LEED analysis of diamond surface characterisation, independent of whether the surface is rough due to etching, or smooth.

Raman Spectroscopy

Determination of sp^2/sp^3 carbon ratio on the surface of the diamond can be conducted using Raman spectroscopy. This technique is effective and non-destructive when characterising surface graphitisation of diamond surfaces[80]. Irradiation of monochromatic light onto a sample induces an electric dipole within molecules due to polarisation of atoms. Oscillation of the induced dipole occurs at the same frequency as the external electromagnetic field, acting as a radiation source for an electromagnetic field scattered in all directions[81]. The intensity of an induced dipole oscillating with frequency (ω) emitting radiation along an angle (θ) is given by **equation 7:**

$$I = \frac{\omega^4 \mu_0^2 \sin^2\theta}{32\pi^2 \epsilon_0 c^3} \quad (7)$$

Where I is the intensity of an induced dipole, ω is frequency, μ_0 is amplitude of the induced electric dipole, ϵ_0 is the permittivity of free space, and c is the speed of light in a vacuum.

Scattering of incident light can be categorised according to the energy changes that are measured between the incident light and the scattered light. If the scattered light remains the same energy as the incidence light, then it is classed as a Rayleigh scattering event, otherwise known as elastic scattering. Scattered light that is lower in energy than the incidence light is classed as Stokes Raman scattering, which occurs when a molecule absorbs this 'lost' energy and becomes excited to the vibrational mode. If the scattered radiation is higher in energy than the incident light, then this will be classed as Anti-Stokes Raman scattering, where the molecule begins the process in an excited vibrational state, and releases energy equal to the molecular vibration, finishing in the ground state [82,83].

The presence of sp^3 -bonded diamond can be confirmed by a single sharp first-order Raman peak a 1332 cm^{-1} in a Raman spectrum, while the presence of graphite on the diamond surface can be confirmed by a peak at 1580 cm^{-1} [84]. There is a lack of literature to support the idea that Raman spectroscopy can be used to determine the composition of terminating species on the surface of the diamond. In fact, there is more evidence to support the fact that Raman spectroscopy is one of the least effective methods of characterising the chemical composition of a functionalised diamond surface, as Raman spectroscopy gives insight into the bulk of the sample being analysed. As the chemical and electronic effects of surface functionalisation spreads to a maximum of only a few nanometres into the bulk of the diamond, Raman spectroscopy is ideally used to gain insight into the extent of surface graphitisation of functionalised diamond surfaces[85].

Functionalisation techniques

Plasma Treatment

One of the most common methods to functionalise the surface of the diamond is by plasma treatment. Common methods include Corona discharge, and low-pressure discharge[86]. Plasma can be described as a gaseous mixture of oppositely-charged particles with a roughly zero net electrical charge[87]. It is formed by electron-impact ionization or photoionization of neutral atoms and molecules in the feed gas, and there are many ways in which energy is supplied for plasma generation. The first method is by supplying thermal energy, using flames to initiate exothermic chemical reactions of the molecules, and using this energy as the primary source. Utilising the adiabatic compression of the gas is also a suitable method of generating enough heat to produce a plasma. Additionally, supplying a gas reservoir with an energetic neutral beam is also a suitable way of creating and sustaining a plasma. However, the most common method of developing a plasma is by applying an electric field to a neutral gas, which will form a low-temperature plasma, commonly used for technological and technical applications[88]. A summary of the methods mentioned are shown in **Figure 16**.

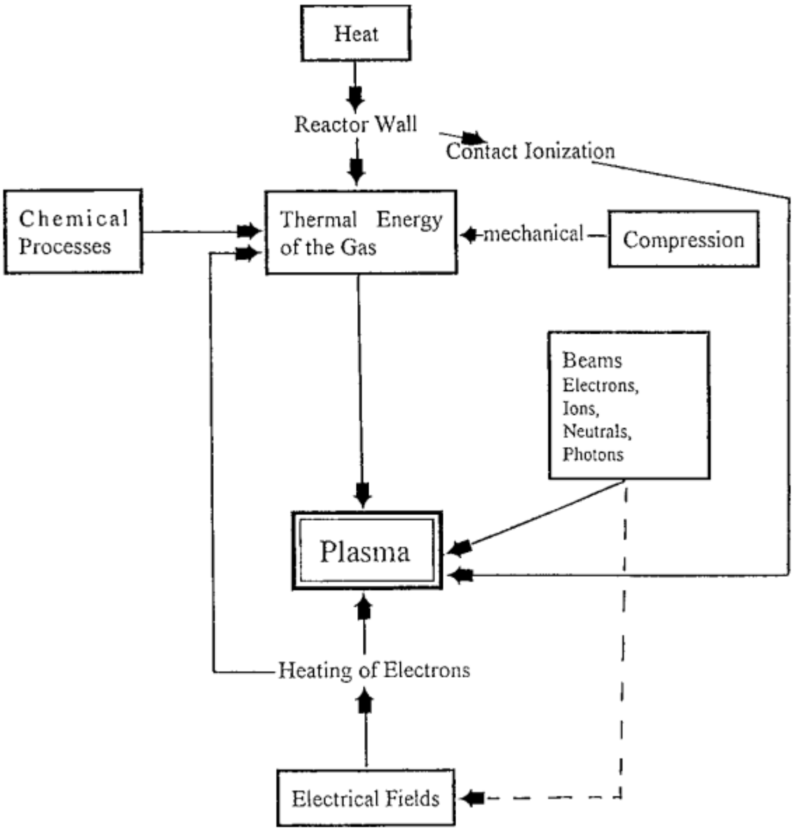

Figure 16 Summary of methods used for energy supply for plasma generation[88]

Dielectric Barrier Discharge Plasma

Dielectric barrier discharge plasma is a low-temperature method of making plasma[89] under atmospheric conditions, removing the need for costly pressure-reducing equipment that many other plasma generation techniques may utilise. Originally, this method was used by Siemens[90] to generate ozone, using a flow of oxygen which was subjected to the influence of a dielectric-barrier discharge. The basis of the dielectric-barrier discharge consists of the presence of one or more insulating layers in the current path between metal electrodes in addition to the discharge space. The dielectric layer acts as a barrier, preventing the direct current from flowing continuously, therefore alternating currents are typically used to drive the discharge. The discharge can have two configurations, as shown in **figure 17**, which shows the planar configuration and the cylindrical configuration. The planar configuration consists of the electrodes and the dielectrics to be arranged in flat, parallel layers, unlike the cylindrical configuration which consists of a cylindrical electrode with a dielectric barrier within it[91].

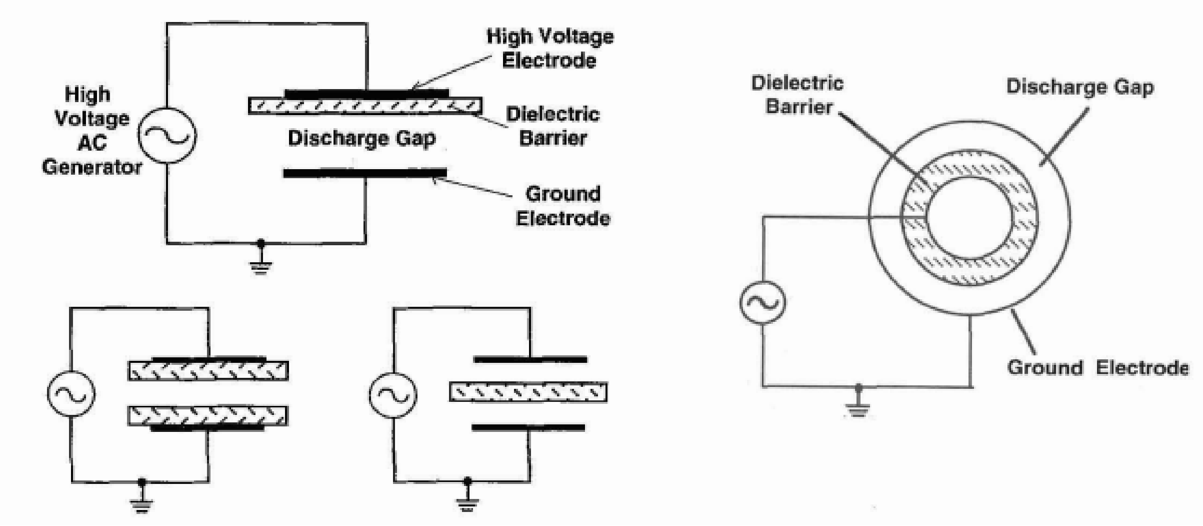

Figure 17 (left) planar discharge configuration, (right) cylindrical configuration[91]

The dielectric barrier discharge plasma treatment can operate under two different regimes, which differentiates this method from other low pressure glow discharges. The filamentary discharge regime is the most common regime, and it is characterised by its short-lived (~10 ns) narrow (~ 100 µm diameter) micro discharges that are evenly and randomly distributed in time and space in the discharge gap of over the dielectric surface. At a macroscopic level, however, discharges form repeatedly at the same location as the polarity of the applied voltage changes, creating a non-uniform deposition. The homogeneous microdischarge-free regime can be subcategorised into glow-like discharges and Townsend-like discharges. Dielectric barrier discharges fed by noble gasses are categorised as glow-like discharges which are formed in the region near the cathode of a positive space charge, producing a strong electric field variation known as a cathode voltage fall. Townsend-like discharges typically occur with when the gas feed is a molecular gas, such as N_2, which produce low-current homogenous discharges. In this scenario, the low ionization level is insignificant, resulting in an electric field that is quasi-uniform over the discharge gap, preventing a cathode fall from developing, which further differentiates between glow-like discharges and Townsend- like discharges[92].

The main advantage of using this method is that it can be conducted under atmospheric pressure and room temperature, eliminating the need to use costly equipment to maintain a reduced pressure atmosphere[93]. On the other hand, this method does require a relatively high voltage of between 1-100 kV, which can be very costly and difficult to supply[94].

Corona Discharge

Corona Discharge is the most utilised method of plasma treatment for surface modification due to the variety of possible electrode configurations that can be used[95]. The discharge is generated by high electric fields at the sharp electrode tip or at the small diameter of a wire[96]. A major advantage of corona discharge is that it is easily formed, however this technique results in non-homogeneous surface treatment, and it cannot be used for thick materials due to the reliance of the system on small inter-electrode spacing (~ 1 mm)[95].

Atmospheric pressure glow discharge and plasma jets

Atmospheric pressure glow discharge (APGD) can create a uniform, homogenous thin film on the desired polymer that is very stable. Its mode of generation is analogous to that of low-pressure glow-discharge, however it has an advantage over filamentary dielectric barrier discharge as it provides a uniform plasma deposition. APPJ is the most recent development in polymer surface treatment and it uses helium and a variety of other gas bends to inhibit arcing. This method is also advantageous over dielectric barrier discharge as it provides a uniform homogenous distribution of plasma. However, APPJ cannot coat the entire material, it can only treat one side of it[95].

Vapour-Phase Oxidation

Previous studies have proven success in the oxidation of diamond surfaces utilising vapour-phase oxidation of diamond powders. The technique involves passing a hydrogenated diamond powder through a tubular flow reactor with the addition of O_2 (20%) in Ar for a variety of temperatures, ranging from 300-1000°C. Characterisation of the product by FTIR, as well as thermal desorption spectra and Raman Spectra were obtained to determine the extent of the oxygen coverage of the diamond surface. Results had shown that the experiment was successful at temperatures between 410-480°C, where the sample was fully terminated with oxygen, and no graphitic or non-diamond residues were detected. Higher temperatures enabled terminal oxygen to desorb from the surface[97].

The study provides useful information on the temperature range at which oxygen chemisorbs onto the surface of diamond, which is useful for future studies. However, this method of surface oxidation would not be a viable method of creating a stable oxide termination for metal-oxide terminated diamond for TEC applications due to the low temperature at which oxygen begins to desorb from the surface of the diamond.

Photochemical Modification

Hydrogen-terminated diamond can be altered under the presence of ultraviolet irradiation (λ=254 nm) with a thin layer of an appropriate protected liquid alkene on the surface. As previously clarified, the H-terminated diamond surfaces possess a negative electron affinity, therefore irradiation of the diamond surface with ultraviolet light photoemits an electron from the surface of the diamond, and the alkene acts as an acceptor molecule. This creates a hole accumulation in the diamond, allowing for the nucleophilic attack at the C-H surface bond by the alkene double bond **(figure 18)**. The wide variety of moieties that can be chemically bonded onto the surface of the diamond proves this method to be highly advantageous, however it is limited by the fact that it cannot be used to create an inorganic termination of the diamond surface, such as an N- or O-termination.

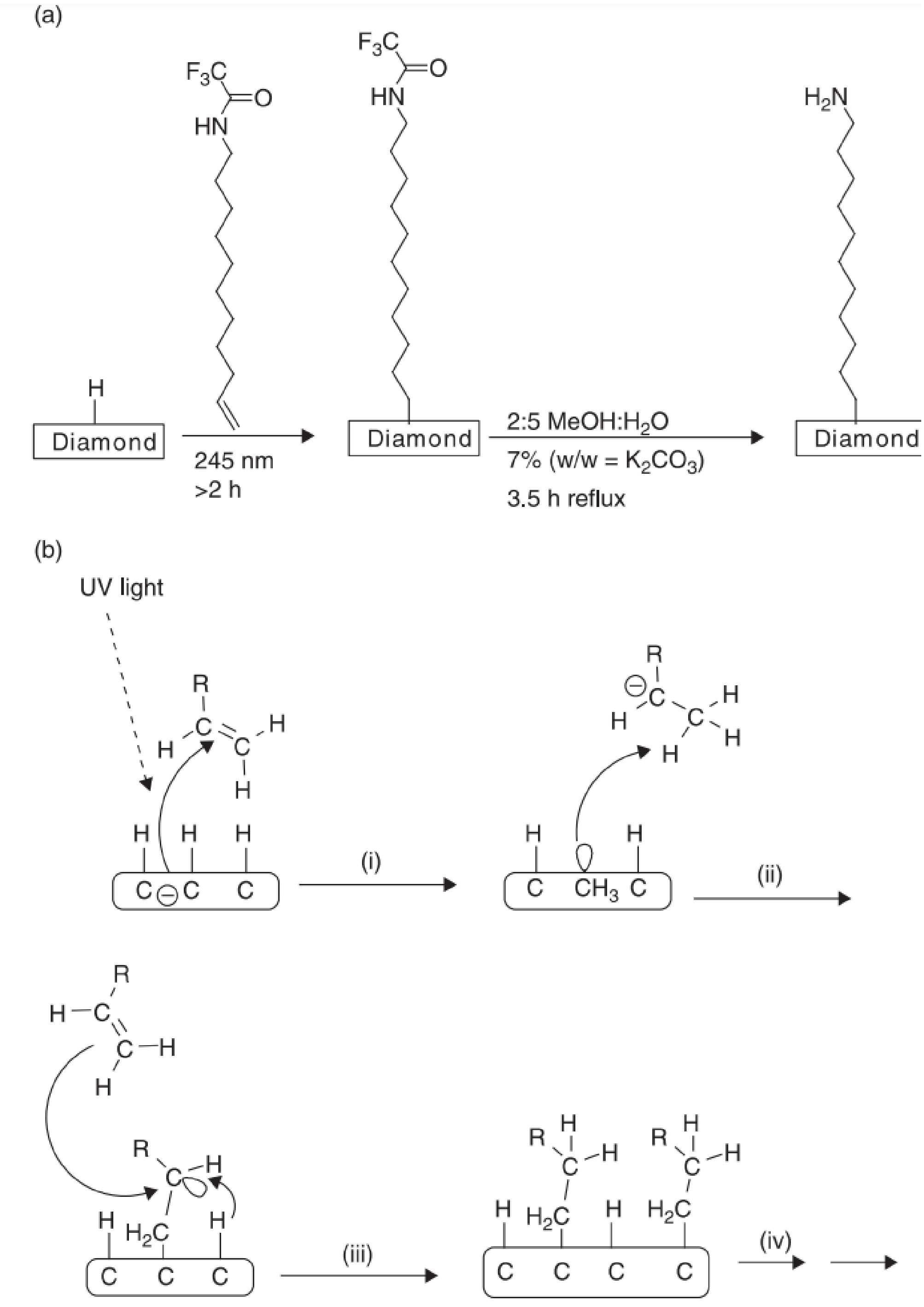

Figure 18 Photochemical modification of the hydrogenated diamond surface[99]

Wet chemical/acid treatment of diamond

Oxidation of the diamond surface can be achieved through acid treatment. Li *et al*[100] compared the effect that different acids and different ratios of acid affected the configuration and extent of oxygen bonding on the surface of microcrystalline diamond powder and polycrystalline diamond film. The method involves submerging the diamond samples in the acid and heating the solution for a certain amount of time (submersion time is dependant on the acid mixture used. Specific experimental conditions can be found in Li's paper.). Analysis of the samples by XPS, FTIR, Raman spectroscopy, and AFM lead to the conclusion that a acid mixture of H_2SO_4/HNO_3 5:1 at 360 °C lead to the best oxygen coverage of the diamond powder (9.6% oxygen coverage) and polycrystalline diamond (9.2% oxygen coverage). Still, the major configuration of oxygen on the surface was the ether configuration (38.9%), with the hydroxyl configuration producing 36.7% of the oxygen coverage, and finally the carbonyl configuration made up 24.4% of the oxygen coverage. It was also found that using a piranha solution for acid treatment gave the highest concentration of hydroxyl terminations for polycrystalline diamond (46.1%), and the second highest for diamond powder (44.1%). Despite not creating the highest oxygen coverage out of all the acid treatments tested, it is more likely to produce hydroxyl terminations, in comparison to other oxygen configurations. Although this is a viable method of surface oxidation, there is still no way to ensure that the oxygen configuration remains consistent across the surface of the diamond. This also leads to the conclusion that the state of the diamond (i.e. powder form or diamond film) will have an effect on the bonding configuration of the oxygen.

UV-Ozone treatment

Oxidation of the diamond surface can be achieved by the UV-ozone process, whereby O_2 is converted ozone via a photochemical reaction, as shown in **equations 8-10.**

$$O_2 + hv \rightarrow 2O^{\bullet} \ (8)$$

$$O_2 + O^{\bullet} \rightarrow O_3 (9)$$

$$O_3 + hv \rightarrow O^{\bullet} + O_2 (10)$$

The resulting oxygen radicals (^1O) commonly creates C=O bonds on the surface of diamond, so long as the diamond is hydrogenated[101]. This is not the case for a dehydrogenated surface that results in the presence of hydroxyl and ether groups on the surface of the diamond[102]. This is likely due to the fact that on a dehydrogenated surface, formation of one C=O π bond is less favourable the formation of two C-O σ bonds[103]. Of course, this method is limited by the lack of control of achieving just one oxygen configuration on the surface of the diamond, despite the lack of C=O carbonyl groups produced on a dehydrogenated surface.

The aforementioned techniques prove to be useful in achieving their respective diamond terminations. However, the techniques used for oxygen terminations lack control of the configuration that oxygen bonds to the diamond surface. None of the techniques result in a homogenous oxide layer, highlighting the need for a method that can achieve a homogenous oxide layer for subsequent metal oxide termination.

Aims of the study

Yoshida *et al*[62] described a method of achieving a fully OH-terminated diamond (100) by use of water vapour annealing. This study aims to replicate these results, as well as achieve a fully N-terminated diamond using SCD diamond (100) and a new tube furnace that had recently been acquired by the University of Bristol CVD Diamond Group, which could be used in place of an oxide layer in metal-oxide terminations. The diamond samples were analysed by XPS at the University of Bristol NanoESCA facility to determine the extent of OH- and N-termination.

Experimental

Commissioning the Tube Furnace for N-termination

The Nabertherm 1200 °C tube furnace was fitted with an N_2 supply on its left side, with an attachment to a vacuum pump on its right, as shown in **Figure 19**. The N_2 supply was controlled by a mass flow controller, measuring N_2 input in sccm, and the vacuum pump was fitted with a digitalised barometer, that controlled the pressure within the tube.

Figure 19 Tube furnace used for N-terminations. On its left is the digital barometer, on its right is the nitrogen input

Under atmospheric conditions with no nitrogen input and no set ramp rate, the tube furnace heated to 1000 °C in the space of 30 minutes and was left to cool overnight to room temperature. Under a reduced pressure of 390 Torr, and a nitrogen flow of 100 sccm, the furnace reached 1000 °C in 40 minutes, and was left overnight to cool to room temperature.

A quartz boat, shown in **Figure 20** was designed to hold a maximum of 3 3x3 mm SCD diamond samples. The boat had to have a flat base to ensure samples lay flat and a height (1.3 cm) that reached just over half the diameter of the quartz tube (2.54 cm), to prevent the boat from rolling over in the furnace. Triangular protrusions were designed to ensure the boat could be pulled out of the furnace with a hook. A repeat of the aforementioned test run was conducted with the quartz boat in the furnace, and the boat successfully remained upright, and was easily inserted and removed with a hook.

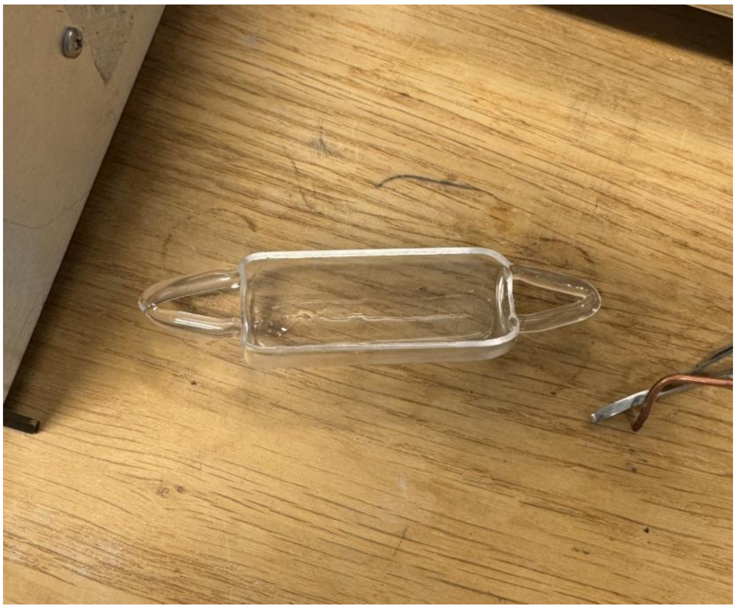

Figure 20 Quartz boat used to hold diamond samples in tube furnace

Acid cleaning of SCD (100) substrates

In order to remove surface impurities from the diamond, the three 3 x 3mm SCD diamond (100) substrates were refluxed in a 100 mL mixture of H_2SO_4 (95%) with 6.5 g of KNO_3. As the temperature approached ~200 °C, nitric acid (HNO_3) was formed *in situ*, providing additional oxidising agents within the sulfuric acid environment. The duration of the treatment was measured from the point that the mixture started to boil, when a yellow hue was observed.

Boron doping of diamond (100) substrates

A conductive boron-doped diamond layer was grown homoepitaxially onto the surface of all diamond substrates by hot-filament chemical vapour deposition (HF-CVD), in order for the substrates to be analysed by XPS. A gas mixture of CH_4 (12.5 sccm) and B_2H_6 (0.65 sccm) in H_2 was used at a pressure of 100 Torr. The backs of the diamond substrates were scratched with a diamond-tipped 'pen'.

N-terminations

All N-terminations were conducted at ½ atmospheric pressure, with a nitrogen flow rate of 500 sccm. A summary of the annealing conditions for samples G1-G3 are shown in **table 1**.

Sample	Temperature (°C)	Hold Time (h)
G1	1000	0
G2	1000	1
G3	600	0

Table 1 Annealing conditions for N-terminations

Diamond samples were placed inside the quartz boat, then pushed into the centre of the tube furnace with a hook. The tube was sealed and the nitrogen flow and reduced atmosphere was applied. The furnace was set to heat to the desired temperature as quick as possible, then hold at that temperature for the desired dwell time, then left to cool to room temperature. The vacuum was turned off, allowing the furnace to regulate to atmospheric pressure. The tube furnace was opened, and the nitrogen flow was increased to >500 sccm. The nitrogen input tube was pointed at the diamond sample while it was being removed and being placed into a sealed vial.

Sample G4

Sample G4 was created after the air leak in the tube furnace was discovered so a slightly different methodology was used. The tube furnace was heated to 900 °C without the quartz boat or diamond sample, using the same nitrogen flow rate as previously mentioned, but at atmospheric pressure. The tube furnace was opened from its right side, and the quartz boat containing the diamond sample was pushed into the centre of the furnace and immediately removed.

OH-termination- samples PM a and PM b

The tube furnace was altered to allow for a flow of N_2+H_2O of nitrogen in the furnace, as depicted in **figure 12**. The OH-terminations were created using the same conditions as samples G1-G3, but at different temperatures, each with a dwell time of 1 hour. Sample PM a was annealed at 700 °C, and sample PM b at 450 °C.

All samples were sealed in a nitrogen-containing vial until analysis.

XPS Analysis

XPS analysis of all diamond samples were performed using a monochromatic Al Kα source (1486.7 eV) at the University of Bristo NanoESCA facility. XPS data was peak fitted analysed using CasaXPS[68], using a Shirley background.

Results and Discussion

N-termination (samples G1-G4)

Samples G1-G3

Nitrogen-termination of the diamond (100) surface was unsuccessful in all reaction conditions. All the samples showed high oxygen content present on the surface of the diamond, with little to no nitrogen content detected by XPS analysis **(see appendix for N-termination XPS data).** Samples G1-G3 were all made before an oxygen leak was detected in the tube furnace, causing significant etching of samples G2 and G3. Sample G2 was almost entirely etched and reduced in size that it was almost invisible to the naked eye. Oxidation of diamond (100) often results in carbonyl termination of the diamond surfaces, and at elevated temperatures, desorption of CO, given by **equation 11**. Desorption of CO results in a point defect on the surface of the diamond, providing a point 'nucleus' for subsequent CO desorption along the (110) direction, leading to a layer-by-layer removal of carbon from the surface of the diamond[104].

$$C_d + {}^{1}\!/_{2}\, O_2 \rightarrow CO \quad (11)$$

Sample G4

This attempted termination was performed after the air leak in the tube furnace was fixed and was performed under a slightly different methodology than samples G1-G3. Instead of heating the tube furnace to 900 °C with the diamond sample inside the tube furnace, and then letting the sample and furnace cool to room temperature in N_2 the furnace was heated to 900 °C without the sample. Then, one end of the tube furnace was opened with the nitrogen flowing through at a high rate (>200 sccm) and the diamond sample was pushed into the middle of the furnace, and then immediately removed. It was then stored in a nitrogen-containing vial until analysis. Despite these slight modifications to the methodology, an insignificant amount of nitrogen content was discovered on the surface of the diamond.

Although complete nitrogen termination was not achieved, our attempts were advantageous as they aided in the discovery of the air leak in the tube furnace. Had the leak in the furnace not been discovered, subsequent attempts of OH-terminations would have been dangerous due to the presence of hydrogen and oxygen present in the tube furnace at temperature >450 °C.

Presence of oxygen on the surface of the attempted N-termination samples can be attributed to stabilisation of the (100) plane by O-termination in comparison to the original H-termination that the diamonds had. A reconstructed 2 × 1 diamond (100) is de-reconstructed into its original 1 × 1 structure when oxygen is bonded to the surface, likely due to oxygens ability to form two C-O bonds by breaking C=C double bonds[105]. At temperatures >800 °C, hydrogen desorbs from the surface of diamond[106], revealing adsorption sites for oxygen atoms. Samples that were not heated to >800°C likely had a weakened C-H bond due to high temperatures, therefore replacement of hydrogen with oxygen may have been thermodynamically favourable. It is this desorption of hydrogen, that makes H-termination unsuitable for TEC applications.

Oxygen present in the air was likely the culprit for the significant amount of oxygen bound to the surface of the diamond. When removing the samples from the tube furnace the samples were exposed to air, despite a high flow of nitrogen (500 sccm) being pointed at the diamond. This highlights the need for the samples to constantly be kept in a nitrogen environment from the point of annealing, until analysis.

Based on these findings, it does not seem possible to anneal nitrogen onto the surface of diamond (100) under the experimental conditions described. This is likely due to the extremely high bond dissociation energy of the N≡N triple bond (941.4 kJ/mol, 9.76 eV)[107], which couldn't be broken in the experimental temperature range.

OH-termination- samples PM a and PM b

Hydroxyl group termination of diamond via water vapour annealing is described by **equation 12**[62]**:**

$$\mathrm{C_{diamond}-H+H_2O(g)\rightarrow C_{diamond}-OH+H_2(g)}(12)$$

As explained earlier, the formation of gaseous hydrogen would have explosive in the scenario that the oxygen leak in the tube furnace had not been discovered, emphasising the importance of conducting a nitrogen-termination

Survey scans

Shown in **figure 21 and 22** is the XPS survey scan of samples PM a and PM b.

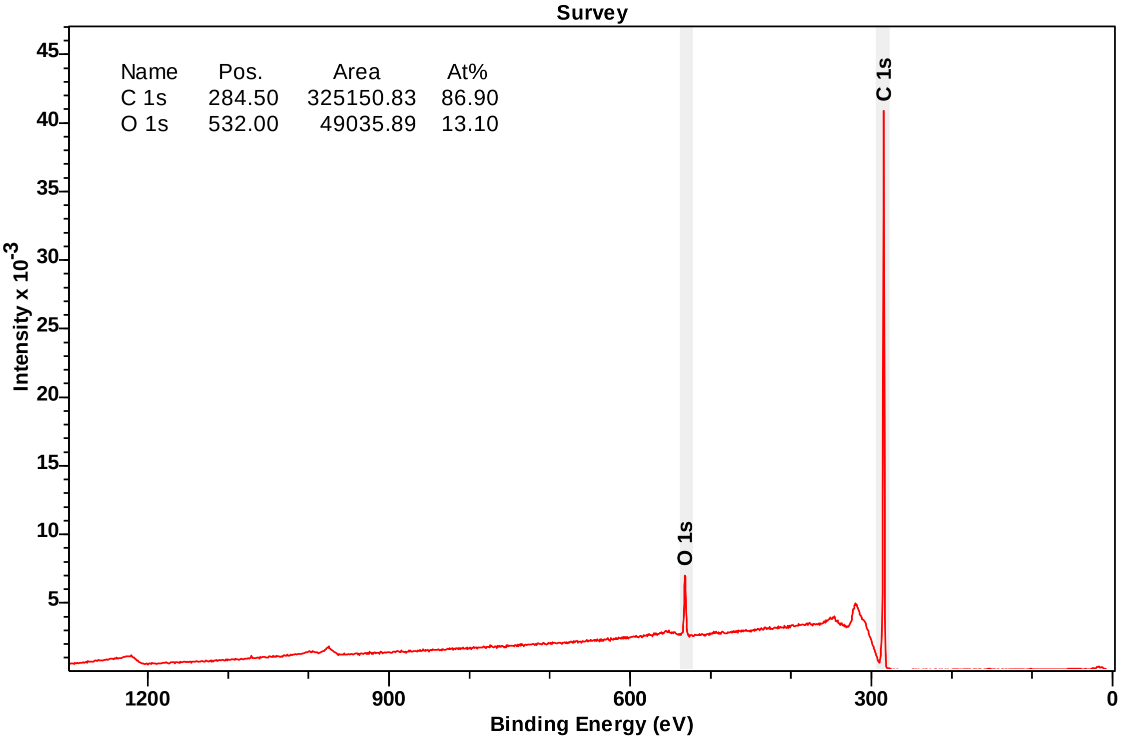

Name	Pos.	Area	At%
C 1s	284.50	325150.83	86.90
O 1s	532.00	49035.89	13.10

Figure 21 XPS survey scan of sample PM a

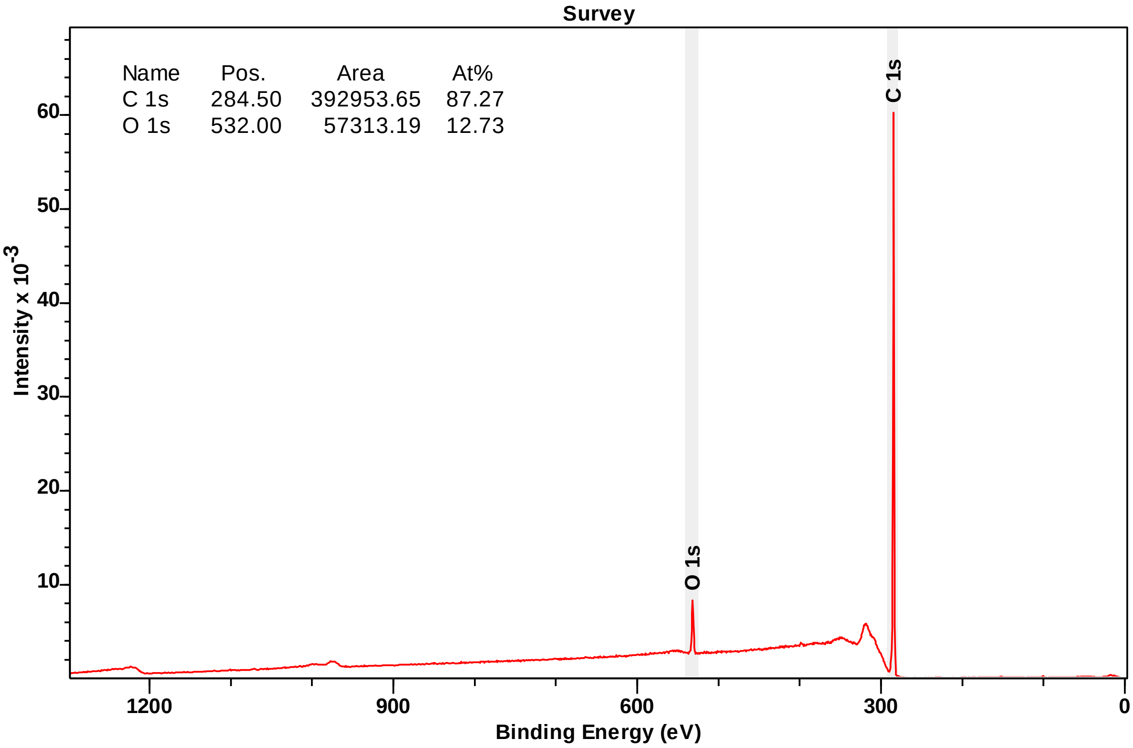

Name	Pos.	Area	At%
C 1s	284.50	392953.65	87.27
O 1s	532.00	57313.19	12.73

Figure 22 XPS survey scan of sample PM b

A survey scan gives a full picture of the elemental species that are present within a 5-10 nm depth of the surface[108]. Characteristic C 1s and O 1s peaks show up at ~284 eV and ~532 eV, which is in agreement with literature values[109]. In both spectra, Auger peaks representing the O KLL transition at ~986 eV and the C KLL transition at ~1221 eV are present, which were identified using the peak library in CasaXPS. This peak arises due to the filling of an emptied K shell, which is filled by a higher energy L shell, releasing energy as it transitions from the L to the K shell. This release of energy gets transferred to another electron in the L shell, which is then ejected as an Auger electron[110].

Deconvolution of the O 1s peak

Deconvolution of the O 1s peaks **(figure 23 and 24)** proceeded with a three-component fit, which resulted in good residual STD values of 0.923 and 1.213 for samples PM a and PM b, respectively. The peaks were fitted with a Shirley background and line profiles were created using a combination of Lorentzian (X%) and Gaussian (Y%) line shapes (GL(X)), where the sum of the two was 100%[109]. It was found that a line profile of GL(35) yielded the closest residual STD value to 1, with residual STD=1 being a perfect fit.

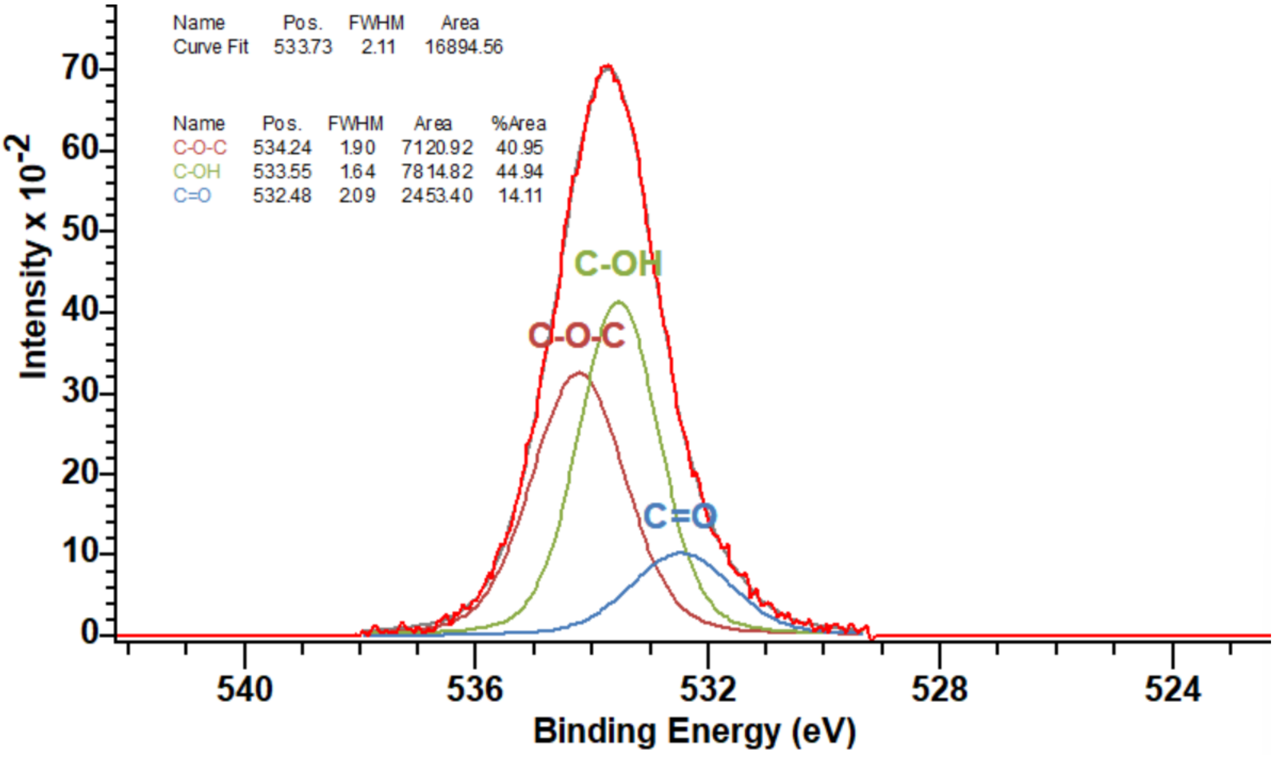

Figure 23 Deconvoluted O 1s peak from sample PM a

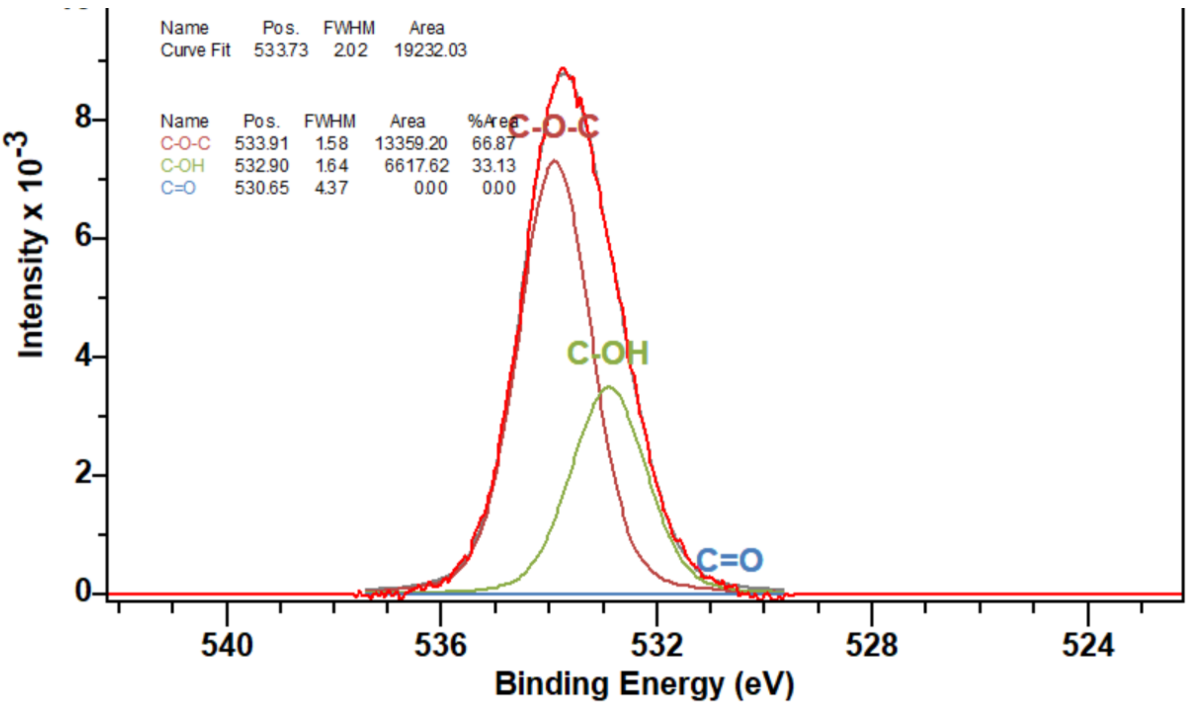

Figure 24 Deconvoluted O 1s peak of samples PM b

Based on literature values [109], the C=O, C-OH, and C-O-C components were centred at ~532 eV, 533 eV, and 534 eV, respectively. The area under the fitted components gives the ratio of the components relative to the total area of the O 1s peak. Based on the deconvoluted O 1s peak, sample PM a had the highest abundance of C-OH bonds (44.94%), followed by C-O-C (40.95%), and C=O (14.11%). Sample PM b gave a lower abundance of C-OH (33.13%), with the major configuration being C-O-C (66.87%), and no C=O bonds present. Dominance of the C-O-C configuration was also seen in studies conducted by Huang *et al*[111] , where a 78% relative abundance of C-O-C on the surface of ultra nanocrystalline diamond after annealing. The results for PM b are inconsistent with Yoshida *et al*[62] study, which claimed to have an absence of the C-O-C signal in the FTIR ATR spectra of the annealed diamond. Though it has been confirmed that the C=O and C-O-C configurations are the most stable on diamond (110)[55], further computational studies of oxygen bonding configurations on the (100) face would need to be conducted, to investigate the configurations' relative stabilities.

Deconvolution of the C 1s peak

Deconvolution of the C 1s peak gives a good insight into the extent of surface graphitisation that had occurred during the annealing process. A two-component peak fitting was conducted on both samples to achieve a residual STD of 3.97 and 3.28 for samples PM a and PM b, respectively. The results from this peak fitting will show some deviance, as indicated by the residual STD values, which indicate that the peak has been underfitted[69]. Nevertheless, the peak fitting should still give a decent insight into the extent of surface graphitisation. The peaks were fitted with GL(30) line shapes which gave the best residual STD. Results for the deconvoluted C 1s spectra are shown in **figure 25 and 26**.

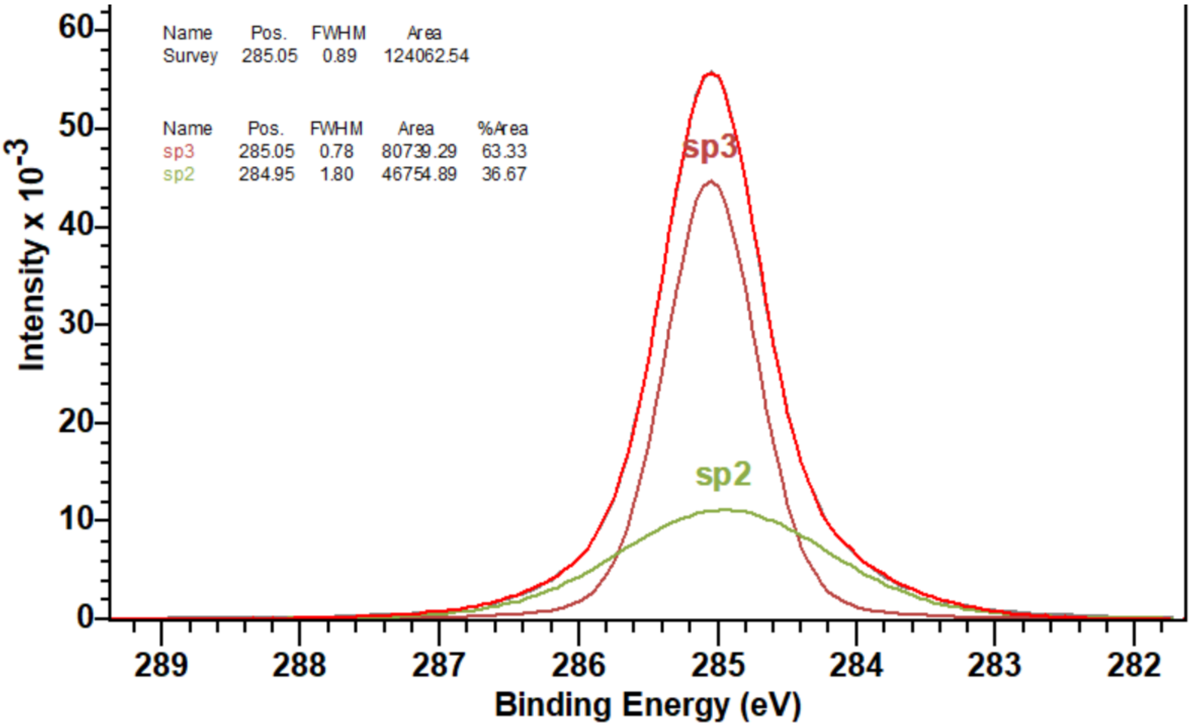

Figure 25 Deconvoluted C 1s peak for PM a

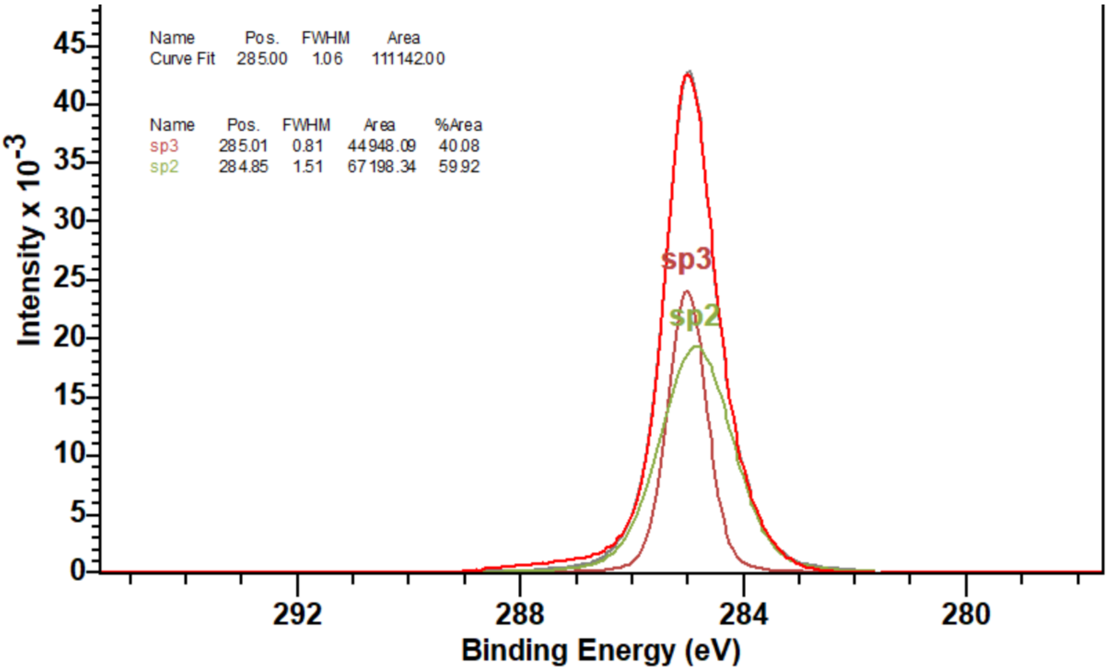

Figure 26 Deconvoluted C 1s peak for sample PM b

The peak positions for sp^3 and sp^2 hybridised carbon were compared against literature values, which indicate that sp^3 hybridised carbon would show a peak at ~285 eV, with the sp^2 peak appearing as a slightly lower binding energy peak at ~284.5 eV[112]. Based on this peak-fitting, sample PM b was graphitised to a greater extent (59.2%) than PM a, whose surface was 36.67% graphitised. These results are surprising as sample PM b showed no C=O bonds on the surface, which would lead to the expectation that the sample would have less surface graphitisation. However, this assumption fails to account for the π bonds that could have formed between surface carbon atoms. It is important to note that the conclusions drawn from this deconvolution are obtained with high uncertainty, due to underfitting of the peak, resulting in a high residual STD.

Surface coverage of oxygen

The extent of surface coverage of oxygen on the annealed diamond can be calculated using **equation(13)**[109], which assumes a uniform oxygen distribution across the diamond surface**:**

$$O\% = \frac{A(O_{1s})/F(O_{1s})}{[\frac{A(O_{1s})}{F(O_{1s})} + \frac{A(C_{1s})}{F(C_{1s})}]} \times 100\% (13)$$

Where A represents the total area of the peak, and F(O_{1s}) and F(C_{1s}) are 0.632 and 0.205 respectively.

Relevant peak areas for both samples are given in **table 2**.

	A(O_{1s})	**A(C_{1s})**
PM a	49035.89	325150.8
PM b	57313.19	392953.7

Table 2 Relevant peak areas of samples PM a and PM b

Using **equation 13**, sample PM a had an oxygen surface coverage of 4.7%, and sample PM b had a coverage of 4.5%. This indicates that the temperature at which the diamonds were annealed at has extremely little effect on the extent of oxygen surface coverage for diamond, at least for the (100) face.

Future Research

In order to develop a broader understanding of the conditions required to achieve a full OH-termination of diamond, the experiments should be repeated under different experimental conditions (i.e. different temperatures and dwell times). By doing so, the optimum conditions required to create a fully OH- or N-terminated diamond can be devised. For example, annealing at temperatures in 100°C intervals would give a very useful insight into the best temperature that achieves complete OH- or N-terminated diamond. It may also be useful to attempt OH- and N-termination on different faces of the diamond, to devise whether this has an effect on surface coverage and bonding configurations. Additional analysis of diamond samples using techniques such as LEED with the ViPErLEED package would be useful in confirming the extent of surface graphitisation of diamonds, to support deconvoluted XPS data. Computational studies of the stabilities of the oxygen configurations on different surfaces of the diamond should be conducted to determine which plane of diamond best favours OH-termination, compares to other oxygen configurations.

Conclusion

To conclude, annealing of the diamond (100) surface with nitrogen is not a viable approach of achieving nitrogen-terminated diamond, at least with the temperatures and dwell times described. Water vapour annealing of the diamond (100) surface is a promising approach of achieving a homogenous OH-terminated diamond surface, however, the study is limited by the sample size of the attempted OH-terminations, as only two annealing conditions were used. Nevertheless, water vapour annealing at 700 °C gave the highest relative abundance of OH-termination, compared to C=O and C-O-C terminations. Surface graphitisation results derived from this study are uncertain, due to high variations in residual STD values, highlighting the importance of accurate peak fitting of the C 1s peak of XPS spectra. The extent of oxygen coverage on the surface of the diamond is not influenced by the temperature at which the diamond is annealed at. The results were not entirely in line with the Yoshida *et al*[62] study, however it should be noted that Yoshida terminated on the (111) face, so the results from this study may differ.

References

1. M. C. James, F. Fogarty, R. Zulkharnay, N. A. Fox, P. May, A review of surface functionalisation of diamond for thermionic emission applications, *Carbon*, 2021, 532-550
2. W. Yarbrough, R. Messier, Current Issues and Problems in the Chemical Vapour Deposition of Diamond, Science, **247**, 1990, 688-696
3. R. H. Telling, C. J. Pickard, M. C. Payne, J. E. Field, Theoretical Strength and Cleavage of Diamond, Physical Review Letters, **84**, 2000, 5160-5163
4. H. Kanda, T. Ohsawa, O. Fukunaga, I. Sunagawa, Effect of solvent metals upon the morphology of synthetic diamonds, Journal of Crystal Growth, 1989, **94**, 115-124
5. Z. ChuanYi, L. Ming, C. LunJian, Growth and characterization of large, high quality cubic diamond crystals, Chinese Science Bulletin, 2012, **57**, 1733-1738
6. N. Yang, Novel Aspects of Diamond, Springer, Berlin, 2015
7. P. Atkins, J. De Paula, and J. Keeler, in *Atkins' Physical Chemistry*, Oxford University Press, Oxford, 12th edition, 2022, ch 15E, 686-700
8. C. Wort, R. Balmer, Diamond as an electronic material, *Materials Today*, **11**, 2008, 22-28
9. A. Kahn, Fermi level, work function and vacuum level, *Material Horizons*, **3**, 2016, 7-10
10. Z. Zhang, J. Yates, Band Bending in Semiconductors: Chemical and Physical Consequences at Surfaces and Interfaces, *Chemical Reviews*, **112**, 2012, 5520-5551
11. J. Macpherson, A practical guide to using boron doped diamond in electrochemical research, *Phys. Chem. Chem. Phys*., **17**, 2015, 2935-2949
12. R. Kalish, Doping of Diamond, *Carbon*, **37**, 1999, 781-785
13. R. Kalish, Ion-implementation in diamond and diamond films: doping, damage effects and their applications, *Applied Surface Science*, **117/118**, 1997, 558-569
14. R. Kalish, C. Uzan-Saguy, B. Philosoph, V. Richter, J. Lagrange, E. Gheeraert, A. Deneuville, A. Collins, Nitrogen doping of diamond by ion implantation, *Diamond and Related Materials*, **6**, 1997, 516-520

15. R, Rouzbahani, K. Jothiramalingam Sankran, P. Pobedinskas, K. Haenen, Advances in n-Type Chemical Vapour Deposition Diamond Growth: Morphology and Dopant Control, *Accounts of Materials Research*, **5**, 2024, 775-785
16. P. Atkins, J. De Paula, and J. Keeler, in *Atkins' Physical Chemistry*, Oxford University Press, Oxford, 12th edition, 2022, ch 15C, 593-599
17. D. Zhu, J. Bandy, S. Li, R. Hamers, Amino-terminated diamond surface: Photoelectron emission and photocatalytic properties, *Surface Science*, 2016, 650, 295-301
18. P. K. Baumann, R. J. Nemanich, Electron affinity and Schottky barrier height of metal-diamond (100), (111), and (110) interfaces, *Journal of Applied Physics*, 1997, 83, 2072-2082
19. C. Li, E. Oliveria, X. Zhang, A. Biswas, S. Roy, A. Puthirath, D. Ruzmetov, M. Neupane, J. Weil, G. Birdwell, T. Ivanov, T, Terlier, T, Gray, H. Kannan, R, Vajtai, D. Galvao, P. Ajayan, Amination of Boron-Doped Diamond Surfaces, *Chemistry of Materials*, 2022, 34, 7190-7200
20. A. Artemenko, H. Kozak, H. Bierderman, A. Choukourov, A. Kromka, Amination of NCD Films for Possible Application in Biosensing, *Plasma Processes and Polymers*, 2015, 12, 336-346
21. S. Rastogi, A. Kalmykov, N. Johnson, T. Cohen-Karni, Bioelectronics with nanocarbons, *Journal of Materials Chemistry B*, 2018, 6, 7159-7178
22. R. Manai, E. Scorsone, L. Rosseau, F. Ghassemi, M. Possas Abreu, G. Lissorgues, N. Tremillion, H. Ginisty, J-C. Arnault, E. Tuccori, M. Bernabei, K. Cali, K.C. Persaud, P. Bergonzo, Grafting odorant binding proteins on diamond bio-MEMS, *Biosensors and Bioelectronics*, 2014, 60, 311-317
23. E. Fontananova, G. Di Profio, L. Giorno, E. Drioli, Membranes and Interfaces Charecterization by Impedance Spectroscopy, *Comprehensive Membrane Science and Engineering II*, 2017, 2, 393-410
24. Y-F. Wang, W. Wang, J. Wei, B. Jiao, D. Xu, X. Chang, H. Abbasi, W. Song, G. Chen, H-X. Wang, Electrochemical route to bio-compatible fluorine-terminated diamond surface, *Carbon*, 2021, 176, 83-87
25. W. Shen, G. Wu, L. Li, H. Li. S. Liu, S. Shen, D. Zou, fluorine-terminated diamond (110) surfaces for nitrogen-vacancy quantum sensors, *Carbon*, 2022, 193, 17-25
26. C. Li, X. Jiang, N. Yang, Synthesis, Surface Chemistry, and Applications of Non-Zero-Dimensional Diamond Nanostructures, *Small*, 2024, 20, 2400798
27. J. Arnault, H. Girard, Hydrogenated nanodiamonds: Synthesis and surface properties, *Current Opinion in Solid State and Materials Science*, 2017, 21, 10-16
28. W. Shen, Y. Pan, S. Shen, H. Lui, Y. Zhang, G. Zhang, Electron affinity of boron-terminated diamond (001) surfaces: a density functional theory study, Journal of Materials Chemistry C, 2019, 7, 9756-9765
29. C. Widmann, C. Giese, M. Wolfer, S. Kono, C. Nebel, F- and Cl-terminations of (100) oriented single crystal diamond, 2014, 211, 2328-2332
30. K. Govindaraju, *et al*, Ultrathin Boron Growth onto Nanodiamond Surfaces via Electrophilic Boron Precursors, *Nanomaterials*, 2024, 14, 1274

31. I. Rojo, F. Texidor, C. Vinas, R. Kivekas, R. Sillanpaa, Relevance of Electronegativity of Boron in η^5-Coordinating Ligands: Regioselective Monoalylation and Monoarylation in Cobalabisdicarbollide $[3,3'\text{-Co}(1,2\text{-}C_2B_9H_{11})_2]^-$ Clusters, *Chem. Eur. J.*, 2003, 9, 4311-4323
32. W. Shen, S. Shen, S. Liu, H. Li, Z. Gan, Q. Zhang, Monolayer Cubic Boron Nitride Terminated Diamond (111) Surfaces for Quantum Sensing and Electron Emission Applications, *Applied Materials & Interfaces*, 2020, 12, 33336-33345
33. K. M. O'Donnell, T. L. Martin, N. L. Allan, Light metals on Oxygen-Terminated Diamond (100): Structure and Electronic Properties, *Chemistry of Materials*, 2015, 27, 1306-1315
34. K. M. Donnell, M. T. Edmonds, A. Tadich, L. Thomsen, A. Stacey, A. Schenk, C. I. Pakes, L. Ley, Extremely high negative electron affinity of diamond via magnesium adsorption, *Physical Review B*, 2015, 92, 035303
35. F. Fogarty, N. A. Fox, P. W. May, Experimental studies of electron affinity and work function from titanium on oxidized diamond (100) surfaces, *Functional Diamond*, 2022, 2, 103-111
36. R. Zulkharnay, N. A. Fox, P. W. May, Enhanced Electron Emission Performance and Air-Surface Stability in ScO-terminated diamond for Thermionic Energy Converters, Small, 2024, 20, 2405408
37. L. Mosinska, P. Popielarski, K. Fabisiak, A. Dychalska, Effects of hydrogen termination of CVD diamond layers, *Optical Materials*, **101**, 2020, 109676
38. D. Takeuchi, H. Kato, G. Ri, T. Yamada, P. Vinod, D. Hwang, C. Nebel, H. Okushi, S. Yamasaki, Direct observation of negative electron affinity in hydrogen-terminated diamond surfaces, *Applied Physics Letters*, **86**, 2005, 152103
39. J. Raymakers, K. Haenen, W. Maes, Diamond surface functionalization: from gemstone to photoelectrochemical applications, *Journal of Materials Chemistry*, **7**, 2019, 10134-10165
40. M. Rutter, J. Robertson, *Ab initio* calculation of electron affinities of diamond surfaces, *Physical Review B*, **57**, 1998, 9241-9245
41. C. Pakes, J. Garrido, H. Kawarada, Diamond surface conductivity: Properties, Devices, and sensors, *Mrs Bulletin*, **39**, 2014, 542-548
42. O. Williams, R. Jackman, Surface conductivity on hydrogen terminated diamond, *Semiconductor Science and Technology*, **18**, 2003, 34-40
43. J. Ristein, M. Riedel, L. Ley, Electrochemical Surface Transfer Doping: The Mechanism Behind the Surface Conductivity of Hydrogen-Terminated Diamond, *Journal of The Electrochemical Society*, **151**, 2004, 315-321
44. J. Chou, A. Retzker, A. Gali, Nitrogen-Terminated Diamond (111) surface for Room-Temperature Quantum Sensing and Simulation, *Nano. Lett*, 17, 2017, 2294-2298
45. M. Gong, Q. Wang, N. Gao, H. Li, Structural and electronic properties of nitrogen-terminated diamond (100) surfaces, *Diamond & Related Materials*, 120, 108601
46. M. Capelli, A. Heffernan, T. Ohshima, H. Abe, J. Jeske, A. Hope, A. Greentree, P. Reineck, B. Gibson, Increased nitrogen-vacancy centre creation yield in diamond through electron beam irradiation at high temperature, *Carbon*, 143, 2019, 714-719

47. A. Gali, *Ab initio* theory of the nitrogen-vacancy centre in diamond, *Nanophotonics*, 8, 2019, 1907-1943
48. M. Doherty, N. Manson, P. Delaney, L. Hollenberg, The negatively charged nitrogen-vacancy centre: the electronic solution, *New Journal of Physics*, 13, 2011, 025019
49. S. Kawai, *et Al*, Nitrogen-Terminated Diamond Surface for Nanoscale NMR by Shallow Nitrogen-Vacancy Centres, *Journal of Physical Chemistry*, 123, 3594-3604
50. B. Myers, A. Das, M. Dartialih, K. Ohno, D. Awschalom, A. Blezxynski Jayich, Probing Surface Noise with Depth-Calibrated Spins in Diamond, *Physical Review Letters*, 113, 2014, 027602
51. B. Ofori-Okai, S. Pezzagna, K. Chang, M. Loretz, R. Schirhagl, Y. Tao, B. Moores, K. Groot-Berning, J. Meijer, C. Degen, Spin properties of very shallow nitrogen vacancy defects in diamond, *Physical Review B*, 86, 2012, 081406
52. S. Sangtawesin, *et al*, Origins of Diamond Surface Noise Probed by Correlating Single-Spin Measurements with Surface Spectroscopy, *Physical Review X*, 9, 2019, 031052
53. E. Janitz, K. Herb, L. Volker, W. Huxter, C, Degen, J. Abendroth, Diamond surface engineering for molecular sensing with nitrogen-vacancy centers, *J. Mater. Chem. C*, 10, 2022, 13533-13569
54. Z. Sun, P. Liang, Q. Liu, B. Cui, N. Gao, Hydrogen and oxygen mixed-termination for nitrogen-vacancy quantum sensors in hexagonal diamond, *Vacuum*, **219**, 2024, 112719
55. S. Chaudari, S. Hall, B. Klein, M. Walker, A. Logsdail, J. Macpherson, R. Maurer, Coexistence of carbonyl and ether groups on oxygen-terminated (110)-oriented diamond surfaces, *Communications materials*, **3**, 2022, 02200228
56. M. Hassan, K. Larsson, Effect of Surface Termination on Diamond (100) Surface Electrochemistry, *Physical Chemistry*, **118**, 2014, 22995-23002
57. D. Petrini, K. Larsson, A Theoretical Study of the Energetic Stability and Geometry of Hydrogen- and Oxygen-Terminated Diamond (100) surfaces, *J. Phys. Chem. C*, **111**, 2007, 795-801
58. X. Zheng, P. Smith, The Stable Configuration for Oxygen Chemisorption on the Diamond (100) and (111) surfaces, *Surface Science*, **262**, 1992, 219-234
59. K. O'Donnell, T. Martin, N. Fox, D. Cherns, *Ab initio* investigation of lithium on the diamond C(100) surface, *Physical Review B*, **82**, 2010, 115303
60. M. James, M. Cattelan, N. Fox, R. Silva, R. Silva, P. May, Experimental Studies of Electron Affinity and Work Function from Aluminium on Oxidized Diamond (100) and (111) Surfaces, *Phys. Status Solidi B*, **258**, 2021, 2100027
61. F. N. Li, Y. Li, H. W. Bao, H. X. Wang, F. Ma, Fabrication of hydroxyl terminated diamond by high-voltage hydroxide ion treatments, *Applied Surface Science*, 2023, 622, 156909
62. R. Yoshida, D. Miyata, T. Makino, S. Yamasaki, T. Matsumoto, T. Inokuma, N. Tokuda, Formation of atomically flat hydroxyl-terminated diamond (111) surfaces via water vapour annealing, *Applied Surface Science*, 2018, 458, 222-225

63. D. Bekas, K. Tsirka, A. Baltzis, A. Paipetis, Self- healing materials: A review of advances in materials, evaluation, charecterization and monitoring techniques, Composites Part B, 2016, **87**, 92-119
64. R. Johnston, Metal Nanoparticles and Nanoalloys, Frontiers of Nanoscience, 2012, **3**, 1-42
65. F. Stevie, C. Donley, Introduction to X-ray photoelectron spectroscopy, Journal of Vacuum Science & Technology, 2020, **38**, 0063204
66. T. Gengenbach, G. Major, M. Linford, C. Easton, Practical guides for x-ray photoelectron spectroscopy (XPS): Interpreting the carbon 1s spectrum, Journal of Vacuum Science and Technology, 2021, **39**, 013204
67. J. C. Lascovich, S. Scaglione, Comparison among XAES, PELS and XPS techniques for evaluation of sp^2 percentage in a-C:H, Applied Surface Science, 1994, **78**, 17-23
68. N. Fairley, CasaXPS: Spectrum Processing Software for XPS, AES and SIMS, Version 2.3.17, Casa Software Ltd, Teignmouth, 2009
69. J. W.Pinder, G. H. Major, D. Baer, J. Terry, J. Whitten, J. Cechal, J. D. Crossman, A. J. Lizarbe, S. Jafari, C. Easton, J. Baltrusaitas, M. van Spronsen, M. Linford, Avoiding common errors in X-ray photoelectron spectroscopy data collection and analysis, and properly reporting instrument parameters, Applied Surface Science Advances, 2024, **19**, 100534
70. J. Whitten, Ultraviolet Photoelectron Spectroscopy: Practical aspects and best practices, Applied Surface Science Advances, 2023, **13**, 100384
71. O. Romanyuk, I. Bartos, I. Gordeev, A. Artemenko, M. Varga, T. Izak, M. Marton, P. Jiricek, A. Kromka, Electron affinity of undoped and boron-doped polycrystalline diamond films, Diamond & Related Materials, 2018, **87**, 208-214
72. G. Wan, M. Cattelan, N. A. Fox, Electronic Structure Tunability of Diamond by Surface Functionalisation, Journal of Physical Chemistry C, 2019, **123**, 4168-4177
73. G. Attard, C. Barnes, in Surfaces, Oxford University Press, New York, 1, 1998, ch 2, 37-82
74. G. Qian, Y. Li, A. R. Gerson, Applications of surface analytical techniques in Earth Sciences, Surface Science Reports, 2015, **70**, 86-133
75. F. Kraushofer, A. M. Imre, G. Franceschi, T. Kiβlinger, E. Rheinfrank, M. Schmid, U. Diebold, L. Hammer, M. Riva, ViPErLEED package I: Calculation of I(V) curves and structural optimization, Physical Review Research, 2025, **7**, 013005
76. E. Soares, C. M. C. de Castilho, V. E. de Carvalho, Advances on surface structural determination by LEED, Journal of Physics: Condensed Matter, 2011, **23**, 303001
77. J. B. Pendry, Multiple scattering theory of electron diffraction, Surface Science, 1994, **299-300**, 375-390
78. W. Moritz, M. A. Van Hove, in Surface Structure Determination by LEED and X-rays, Cambridge University Press, Cambridge, 1, 2022, ch 1, 1-5
79. G. Held, Structure determination by low-energy electron diffraction-A roadmap to the future, Surface Science, 2025, **754**, 122696
80. S. Prawer, R. J. Nemanich, Raman spectroscopy of diamond and doped diamond, Philosophical Transaction of the Royal Society A, 2004, **362**, 2537-2565
81. D. Cialla-May, M. Schmitt, J. Popp, Theoretical principles of Raman spectroscopy, Physical Science Reviews, 2019, **4**
82. D. W. Shipp, F. Sinjab, I. Notingher, Raman spectroscopy: techniques and applications in the life science, Advances in Optics and Photonics, 2017, **9**, 318-398
83. J. Luong, K. Male, J. Glennon, Boron-doped diamond electrode: synthesis, charecterization, functionalization and analytical applications, Analyst, 2009, **134**, 1965-1979

84. A. Puthirath, E. Oliveira, G. Gao, N. Chakingal, H. Kannan, C. Li, X. Zhang, A. Biswas, M. Neupane, B. Pate, D. Ruzmetov, A. Birdwell, T. Ivanov, D. Galvao, R. Vajtai, P. Ajayan, Oxygenation of Diamond Surfaces via Hummer's method, Chemistry of Materials, 2021, **33**, 4977-4987
85. G. Barnes, I. Gentle, in Interfacial Science: An Introduction, Oxford University Press, New York, 2, 2011, ch 7, 182-200
86. E. Liston, L. Martinu, M. Wertheimer, Plasma surface modification of polymers for improved adhesion: a critical review, *J. Adhesion Sci Technol.*, 1993, **7,** 1091-1127
87. F. Denes, S. Manolache, Macromolecular plasma-chemistry: an emerging field of polymer science, *Progress in Polymer Science*, 2004, **29**, 815-885
88. H. Conrads, M. Schmidt, Plasma generation and plasma sources, *Plasma Sources Sci. Technol.*, 2000, **9**, 441-454
89. L. Zhu, S. Wang, L. Zhao, X. Li, Dielectric barrier discharge low-temperature plasma modification of bamboo charcoal for supercapacitor applications, *Biosource Technology*, 2024, **411**, 131287
90. U. Kogelschatz, Dielectric-barrier Discharges: Their History, Discharge Physcis, and Industrial Applications. *Plasma Chemistry and Plasma Processing*, 2003, **23**, 1-46
91. U. Kogelschatz, B. Eliasson, W. Egli, Dielectric-Barrier Discharges. Principle and Applications, *Journal de physique IV Proceedings*, 1997, **7**, 47-66
92. F. Fanelli, Thin film deposition and surface modification with atmospheric pressure dielectric barrier discharges, *Surface & Coatings Technology*, 2010, **205**, 1536-1543
93. J. He, X. Wen, L. Wu, H. Chen, J. Hu, X. Hou, Dielectric barrier discharge plasma for nanomaterials: Fabrication, modification and analytical applications, *Trends in Analytical Chemistry*, 2022, **156**, 116715
94. R. Brandenburg, Corrigendum: Dielectric barrier discharges: progress on plasma sources and on the understanding of regimes and single filaments, *Plasma sources Sci, Technol.*, 2017, **26**, 1361
95. R. Abd Jelil, A review of low-temperature plasma treatment of textile materials, *J. Mater. Sci.*, 2015, **50**, 5913-5943
96. Y. Vadikkeettil, Y. Subramaniam, R. Murugan, P. Ananthapadmanabhan, J. Mostaghimi, L. Pershin, C. Batiot-Dupeyrat, Y. Kobayashi, Plasma assisted decomposition and reforming of greenhouse gases: A review of current status and emerging trends, *Renewable and Sustainable Energy Reviews*, 2022, **161**, 112343
97. T. Ando, K. Yamamoto, M. Ishii, M. Kamo, Y. Sato, Vapor-phase Oxidation of Diamond Surfaces in O_2 studies by Diffuse Reflectance Fourier-transfrom infrared and Temperature-programmed Desorption Spectroscopy, *J. Chem. Soc. Faraday Trans*, **89**, 1993, 3635-3640
98. L. Schwaederlé, P. Brault, C. Rond, A. Gicquel, Molecular dynamics calculations of CH_3 sticking coefficient onto diamond surfaces, *Plasma Processes and Polymers*, **12**, 2015, 764-770
99. S. Szunerits, R. Boukherroub, in *Diamond-Based Materials for Biomedical Applications*, Woodhead Publishing Series in Biomaterials, France, 2013, 2, 25-47
100. C. Li, Z. Zhang, E. F. Oliveira, A. B. Puthirath, M. R. Nerupane, J. D. Weil, A. Glen Birdwell, T. G. Ivanov, S. Kong, T. Gray, H. Kannan, A. Biswas, R. Vajtaj, D. S.

Galvao, P. M. Ajayan, Systematic comparison of carious oxidation treatments on diamond surface, *Carbon*, 2021, **182**, 725-734

101. M. Yan, L. Wan, J. Wang, Z. Ma, P. Wang, N. Gao, H. Li, SSurface Ixygen Adsorption and Electric Property of Hydrogen-Terminated Single Crystal Diamonds by UV/ozone Treatment, *Chin. Phys. Lett*, 2020, **37**, 066801
102. R. Boukherrob, X. Wallart, S. Szunerits, B. Marcus, P. Bouvier, M. Mermoux, Photochemical oxidation of hydrogenated boron-doped diamond samples, *Electrochemical Communications*, 2005, **7**, 937-940
103. H. Tamura, H. Zhou, K. Sugissako, Y. Yokoi, M. Kubo, K. Teraishi, A. Miyamoto, Periodic density-functional study on oxidation of diamond (100) surfaces, *Physical Review B*, 2000, **61**, 11025-11033
104. P. John, N. Polwart, C. E. Troupe, J. I. B. Wilson, The oxidation of (100) textured diamond, *Diamond and Related Material*, 2002, **11**, 861-866
105. K. Larsson, *Simulation of Diamond Surface Chemistry: Reactivity and Properties*, IntechOpen, London, 2019
106. M. McGonigal, M. L. Kempel, S. M. Hammond, K.D. Jamison, Isothermal hydrogen desorption from the diamond (100) 2 × 1 surface, *Journal of Vacuum Science & Technology A: Vacuum, Surfaces, and Films*, 1996, **14**, 2308-2314
107. B. Ruscic, D. Feller, K. A. Peterson, Active Thermochemical Tables: dissociation energies of several homonuclear first-row diatomic and related thermochemical values, *Theoretical Chemical Accounts*, 2014, **133**, 1415
108. R. E. Galindo, R. Gago, D. Duday, C. Palacio, Towards nanometric resolution in multilayer depth profiling: a comparative study of RBS, SIMS, XPS and GDOES, *Analytical and Bioanalytical Chemsitry*, 2010, **396**, 2725-2740
109. R. Zulkharnay, G. Zulpukarova, P. W. May, Oxygen-terminated diamond: insights into the correlation between surface oxygen configurations and work functions, *Applied Surface Science*, 2024, **658**, 159776
110. C. Chang, Auger Electron Spectroscopy, *Surface Science,* 1971, **25**, 53-79
111. K. Huang, X. Hu, H. Xu, Y. Shen, A. Khomich, The oxidation behavior and mechanical properties of ultrananocrystalline diamond films at high temperatures using annealing, *Applied Surface Science*, 2014, **317**, 11-18
112. D. J. Morgan, Comments on the XPS Analysis of Carbon Materials, *Journal of Carbon Research*, 2021, **7**, 51
113. E. McCash, *Surface Chemistry*, Oxford University Press, Oxford, 2001
114. S. Ishii, S. Saiki, S. Onoda, Y. Masuyama, H. Abe, T. Ohshima, Ensemble Negatively Charged Nitrogen-Vacancy Canters in Type-Ib Diamond Created by High Fluence Electron Beam Irradiation, *Quantum Beam Sci.*, 2022, **6**, 6010002
115.

Appendix

Sample G1 survey scan

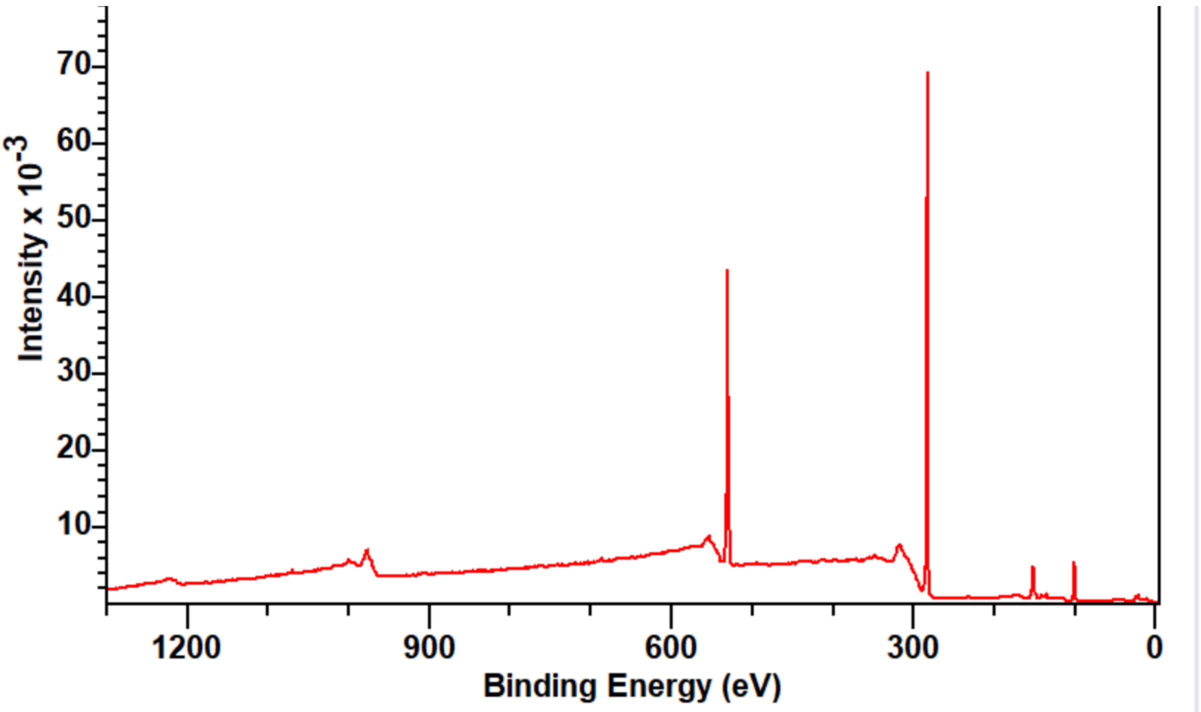

Sample G3 Survey scan

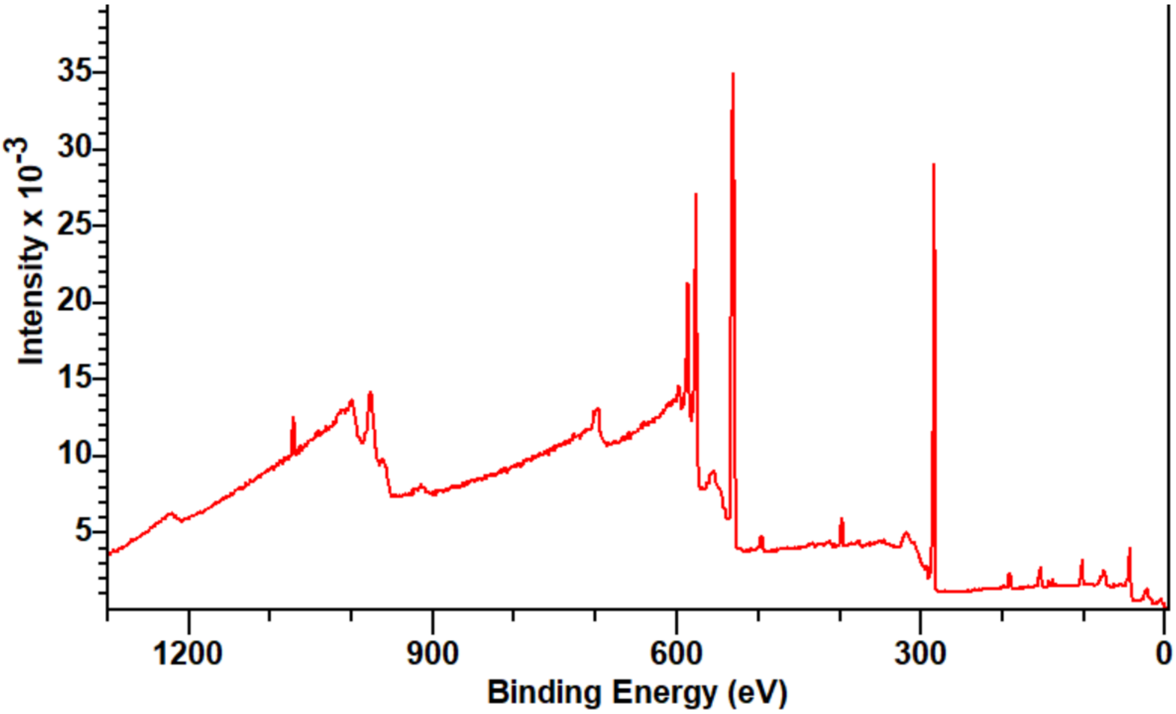

Sample G4 survey scan